

For Reference

NOT TO BE TAKEN FROM THIS ROOM

Ex LIBRIS
UNIVERSITATIS
ALBERTAENSIS



THE UNIVERSITY OF ALBERTA

THE RELATIONSHIP OF SOUTHWARD DRIFTING AURORAL
ARCS TO THE MAGNETOSPHERIC ELECTRIC FIELD AND
SUBSTORM ACTIVITY

by



SAVITHRI SUBBARAO


A THESIS

SUBMITTED TO THE FACULTY OF GRADUATE STUDIES AND RESEARCH
IN PARTIAL FULFILLMENT OF THE REQUIREMENTS FOR THE DEGREE
OF MASTER OF SCIENCE

DEPARTMENT OF PHYSICS

EDMONTON, ALBERTA

FALL, 1972



Digitized by the Internet Archive
in 2023 with funding from
University of Alberta Library

<https://archive.org/details/Subbarao1972>

UNIVERSITY OF ALBERTA

FACULTY OF GRADUATE STUDIES AND RESEARCH

The undersigned certify that they have read, and recommend to the Faculty of Graduate Studies and Research, for acceptance, a thesis entitled THE RELATIONSHIP OF SOUTHWARD DRIFTING AURORAL ARCS TO THE MAGNETOSPHERIC ELECTRIC FIELD AND SUBSTORM ACTIVITY, submitted by Savithri Subbarao in partial fulfillment of the requirements for the degree of Master of Science

ABSTRACT

The magnitude of the westward directed auroral zone electric field is inferred from the measurement of the southward drift of moderately bright auroral arcs. In a sample of 43 events recorded over a period of 15 months at Fort Smith (68.1°N geomagnetic) it was found that southward drifting arcs were predominantly associated with the decay phase of polar magnetic substorms, and no evidence was found for the association of southward drifting arcs with the so-called growth phase of substorms. It is suggested that the southward drifting arcs are generated through the precipitation of energetic plasma affected by the limit on stably trapped particle fluxes proposed by Kennel and Petschek (1966).

ACKNOWLEDGEMENTS

I am very grateful to my supervisor, Dr. G. Postoker and Professor J. A. Jacobs for their encouragement and support throughout the course of this research. I also wish to thank Dr. A. J. Chen and Dr. J. L. Kisabeth for informative discussions, and Mr. D. B. Guptill for developing the computer programs. I particularly wish to thank Dr. R. D. Sharp, of Lockheed Research Laboratories, for pointing out an important theoretical error.

I am indebted to the Atmospheric Environment Service of Canada and the Department of Energy, Mines and Resources for permission to operate the all-sky cameras at Fort Smith and Meanook. This research was supported by the National Research Council of Canada and in part by the Boreal Institute for Northern Studies of the University of Alberta.

TABLE OF CONTENTS

	Page
CHAPTER 1. INTRODUCTION	
1.1 Structure of the Magnetosphere	1
1.2 Drifts of Trapped Charged Particles	3
1.3 The Magnetospheric Substorm	9
1.4 Purpose of Thesis	10
CHAPTER 2. DETAILS OF THE ANALYSIS	
2.1 The All-sky Camera	15
2.2 The Mapping Factor	22
2.3 Magnetic Data	24
CHAPTER 3. PRESENTATION OF THE DATA	
3.1 Observational Results	30
3.2 Sample Events	33
CHAPTER 4. DISCUSSION AND CONCLUSIONS	
4.1 Mozer's Model	52
4.2 The Kennel-Petschek Mechanism	53
4.3 Proposed Mechanism of Auroral Particle Precipitation	55
4.4 Conclusions	62
BIBLIOGRAPHY	64
APPENDIX	A1

LIST OF TABLES

Table		Page
2.1	Co-ordinates of magnetic observatories whose records are used to determine phase of substorm	25
2.2	Co-ordinates of magnetic observatories whose records are used to create latitude profiles	28
3.1	Electric field values inferred from southward drifting arcs	31
3.2	Summary of magnetic correlation	31
A1	List of events	A1
A2	Summary of Results	A23

LIST OF ILLUSTRATIONS

Figure		Page
1.1	The Earth's magnetosphere and tail, as seen in the noon-midnight meridian plane. The dotted lines on the nightside show the dipolar field configuration which would be present in the absence of the solar wind. Distances are marked in units of Earth radii.	2
1.2	The seven stages in the development of the auroral substorm, starting from quiet conditions, through active periods and back to quiet-time conditions. The centre of the concentric circles is the north geomagnetic pole; the sun is towards the top of the diagram. The arrows in the arc forms indicate direction of arc motion (after Akasofu, 1964).	11
1.3	$\mathbf{E} \times \mathbf{B}$ drift of particles shown in the noon-midnight meridian plane under the action of a dawn-to-dusk electric field. Note that the first order drift would be azimuthal while the zeroth order drift is Earthward.	13
2.1	Sample all-sky camera photographs taken at 0420 UT and 0421 UT on October 29, 1971. North is to the right of the camera frame and the centre of the cross-hairs marks the zenith position.	16
2.2	Sample of an ASCA analysis sheet. The projected ASCA image is traced directly onto the sheet.	19
2.3	The auroral arc mapper. The holes give the mapped arc position when the edge point to which it is connected is superposed in the traced arc.	20

Figure		Page
2.4	Auroral arcs recorded on October 29, 1971 (see Figure 2.1) mapped onto a linear scale. The scale covers distances up to 300 km in each direction. Distortion of the arc forms an uncertainty in location increase from the zenith position outward to the edges of the photograph. The scale is 1 inch to 100 km. The universal time for each photograph is marked at the edge of the arc whose motion is being traced.	21
2.5	Locations of the magnetometer stations (double circles) used in the collection of data from which the latitude profiles of the magnetic perturbation pattern are constructed. Solid circles represent standard magnetic observatories whose records were used in the magnetic correlation.	26
3.1a	Two successive latitude profiles taken during an interval of southward drifting arcs recorded on October 9, 1971. The positions of the arcs are indicated by the solid arrows. This type of profile is typical of those associated with evening sector equatorward drift of the arcs. We have a double current system, with the boundary of the eastward and westward electrojets being the site of the development and motion of the arcs.	35
3.1b	The mapped auroral arcs for event 20, whose corresponding latitude profiles appear in Figure 3.1a.	36
3.1c	The mapped auroral arcs for event 21, also corresponding to the profiles of Figure 3.1a. Note the multiple arc structure.	37
3.2a	Latitude profiles for event 22. Note the decrease in D. The arc positions appear to coincide exactly with the boundary of the two electrojets, even as the westward electrojet decreases and the eastward electrojet increases.	38

Figure		Page
3.2b	The corresponding mapped auroral arcs for event 22.	39
3.3a	Latitude profiles of event 23. The double current system associated with event 22 still is present, although the westward electrojet has decreased considerably in intensity compared to that shown in Figure 3.1a. Again, the arcs move south as the boundary of the two electrojets moves equatorward.	40
3.3b	The corresponding mapped arcs for event 23. Note event 24 (Figure 3.4b) starts before event 23 has completely decayed, presenting another example of multiple arcs.	41
3.4a	Differential latitude profiles of event 24, using a baseline established a few minutes prior to the appearance of the arcs. Note that event 24 starts while event 23 is still in progress. This is marked by the sudden increase in the D component at Fort Reliance, indicative of increased convection across the polar cap.	42
3.4b	The corresponding mapped arcs for event 24.	43
3.5a	Latitude profiles for event 25. Note that the arcs follow the equatorward motion of the poleward component of the auroral electrojet system.	44
3.5b	The corresponding mapped arcs for event 25. This is an excellent example of steady southward motion of the arcs.	45
3.6	Differential latitude profiles for event 37. The intensification of the northern component of the electrojet is associated with development of the arc. The arc motion does not seem to be associated with any measureable motion of the electrojet, although the electrojet tends to widen during the period of arc drift. The corresponding mapped arcs for event 37 are shown in Figure 2.4	46

Figure

Page

- 3.7a Differential latitude profiles for event 19. This profile is typical of that for a westward electrojet, except for the very large D component perturbation north of the electrojet. The arc positions coincide with the peak of the ΔH profile. A1
- 3.7b The corresponding mapped arcs for event 19. Note that the first two arcs end just at the zenith. This indicates that the precipitation of auroral electrons may occur in localized azimuthal sectors of an L-shell. A8
- 3.8 Magnetograms from Fort Reliance, Fort Smith, Fort McMurray and Meadeck for October 9, 1971. This day was the most active one observed the period examined; a total of 12 events (events 20 to 31) occurred during this time. A9
- A1(a) Latitude profiles for event 8. The large -D at $\sim 63^\circ N$ indicates a strong poleward flow of current at 0605 UT, which one might expect to find at the westward end of the auroral electrojet. The arcs are situated near the southern border of the auroral oval. The western edge of the auroral electrojet eventually expands the station line, so that by 0610 UT the large -D has disappeared at our meridian. A26
- A1(b) The corresponding mapped arcs for event 8. The times for the arcs are given in local time (UT-7). A17
- A2(a) Latitude profiles for event 14. A weak westward electrojet and a stronger westward jet at a higher latitude influences the magnetic field perturbation pattern. This event is quite similar to event 37 (shown in Figure 3.6(a)). A26
- A2(b) The corresponding mapped arcs for event 14. A19

Figure

Page

A3(a) Latitude profiles for event 31. Here we have a strong westward electrojet with intense poleward and equatorward current flow. The arcs lie near the boundary between the two electrojets.

A30

A3(b) The corresponding mapped arcs for event 31.

A31

A4(a) Differential latitude profiles for event 33. The decrease in the intensity of the westward electrojet to the north has the appearance of equatorward motion.

A32

A4(b) The corresponding mapped arcs for event 33. Note the tilt of the arcs, indicative of a north-south component of electric field, as well as an east-west component.

A33

1. INTRODUCTION

1.1 Structure of the Magnetosphere

The interaction of the solar wind with the Earth's magnetic field results in the distortion of the dipolar structure of the magnetic field, compressing it on the solar side and extending it on the anti-solar side to form the magnetotail. The various parts of the magnetosphere (the name given to the distorted magnetic field configuration) are shown in Figure 1.1. The magnetosphere is populated with energetic charged particles (found mainly in the belts of trapped radiation) and thermal plasma (found in the plasma sheet extending into the magnetotail, and in the plasmasphere).

The particles in the magnetotail experience convective drift motion arising from the gradients in the magnetic field of the tail, as well as from the electric field which is usually directed across the tail from dawn to dusk. The inner boundary of the convection pattern of the particles can also be identified with the boundary of the plasmasphere (termed the plasmopause). The projection of the outer boundary of the trapping region along the geomagnetic field lines to the ionosphere corresponds approximately with the auroral oval, which is defined as the instantaneous locus of auroral activity. This is thought to be the case since the energetic particles in

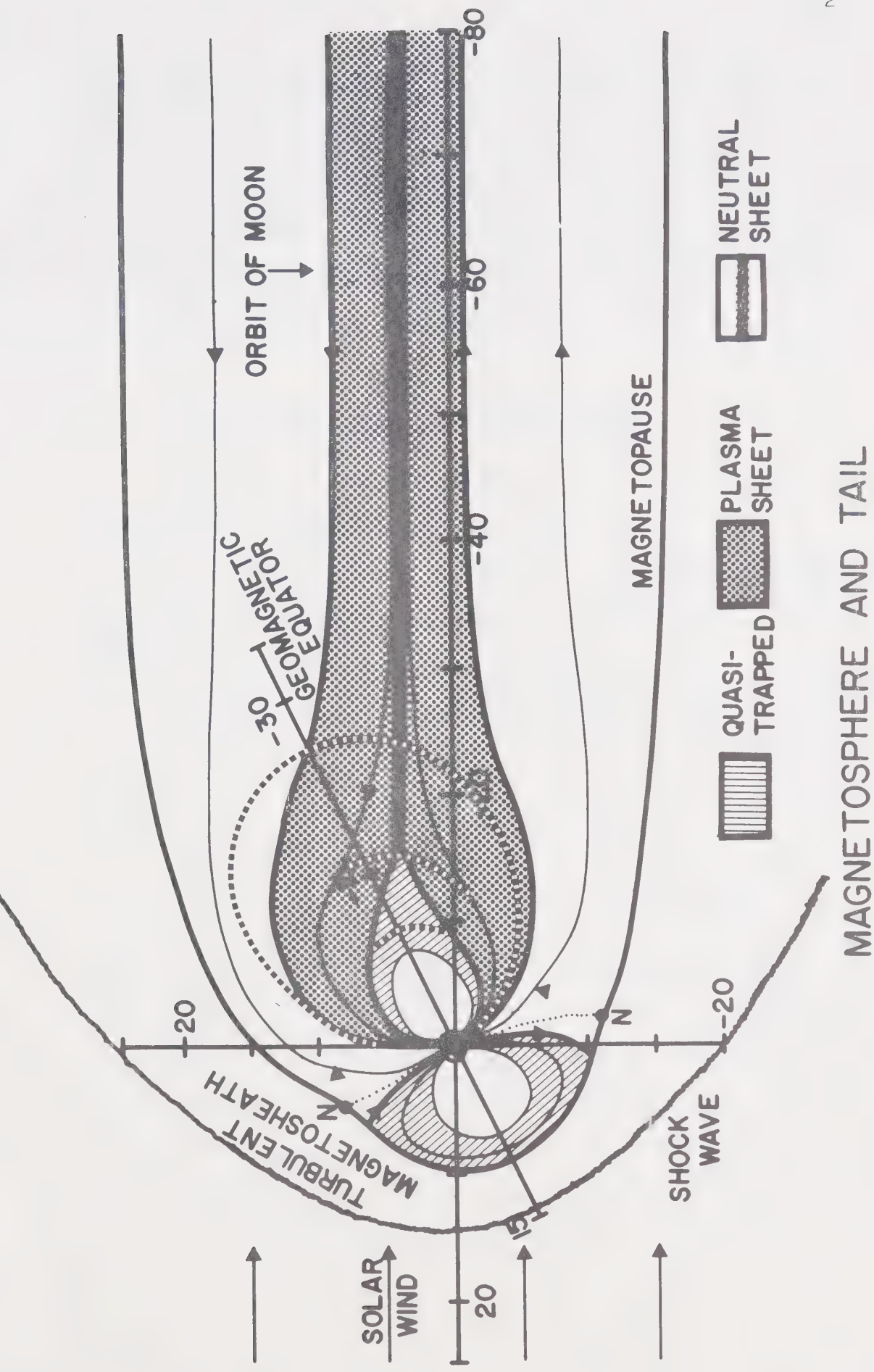


Figure 1.1

the trapping region are the ones that are eventually precipitated to cause auroras. It is important to understand the behaviour of these energetic particles under the action of electric and magnetic fields in order to gain some insight into the method by which auroral activity is generated.

1.2 Drifts of Trapped Charged Particles

Let us now consider the motions to which the trapped particles are subject (Roederer, 1970). A charged particle in the presence of the Earth's magnetic field will in general experience three types of motion, namely, a cyclotron motion, a bounce motion, and a drift motion along a closed surface bounded by field lines. These three types of motion are governed respectively by the first, second, and third adiabatic invariants.

We first consider the cyclotron motion. For the purposes of this discussion we use the guiding centre approximation, and define the guiding centre system (GCS) as a moving frame of reference in which, at any instant of time, an observer sees the particle in a periodic orbit perpendicular to the direction of the magnetic field. The particle's motion can then be described in terms of the displacement of the guiding centre, with the particle in cyclotron motion about the guiding centre; the

instantaneous velocity of the guiding centre is defined to be the velocity of the GCS.

For a particle in a uniform static magnetic field under the influence of an external nonmagnetic force \underline{F} (constant in space and time), the equation of motion can be written as

$$\frac{d\underline{p}_{||}}{dt} = \underline{F}_{||} \quad (1)$$

$$\frac{d\underline{p}_{\perp}}{dt} = \underline{F}_{\perp} + q \underline{V}_{\perp} \times \underline{B} \quad (2)$$

the parallel and perpendicular directions being defined with respect to the magnetic field direction.

The first of these equations gives the parallel velocity of the particle and the GCS, $V_{||}$. The perpendicular, or drift velocity \underline{V}_F of the GCS is given by the instantaneous velocity of a reference frame in which the particle executes its cyclotron motion. In this reference frame, the external force \underline{F}_{\perp}^* ($= \underline{F}_{\perp}$) (starred symbols refer to quantities in the GCS) will be balanced by the induced electric field force:

$$q \underline{E}^* = q \underline{V}_F \times \underline{B} \quad (3)$$

Therefore, we have that :

$$q \underline{V}_F \times \underline{B} = - \underline{F}_{\perp} \quad (4)$$

$$\frac{\underline{B}}{qB^2} \times q(\underline{V}_F \times \underline{B}) = - \frac{\underline{B}}{qB^2} \times \underline{F}_\perp \quad (5)$$

$$\underline{V}_F = \frac{\underline{F}_\perp \times \underline{B}}{qB^2} \quad (6)$$

This is the zeroth order, or force, drift of the particle. Outside the GCS, the particle has a cyclotron motion, a translation with constant velocity \underline{V}_F , and a translation parallel to the field line. Note that equation (6) above is non-relativistic, the condition for its validity being:

$$\frac{F_\perp}{qB} < c \quad (7)$$

If the external force is not constant in space, but is given by the gradient of a scalar potential:

$$\underline{F} = - \nabla U \quad (8)$$

condition (7) becomes:

$$\nabla U \rho_c \ll T \quad (9)$$

where ρ_c is the Larmor radius of the particle, and T its kinetic energy. This leads to the restriction:

$$V_F \ll v \quad (10)$$

where v is the particle's velocity.

Now suppose the particle is in a non-uniform magnetic field. The gradient of the field can also be written as a sum of two components, $\nabla_{\perp} B$ and $\nabla_{\parallel} B$. First consider only the perpendicular gradient. Its effect will be to cause an alternating change of the Larmor radius in the particle's orbit. This change acts in the same way as a net Lorentz force directed oppositely to $\nabla_{\perp} B$. The cyclotron average of this net force, R , is:

$$R = \frac{1}{2} q v_{\perp} \nabla_{\perp} B \rho_c . \quad (11)$$

This force has an associated drift, as has just been derived (eq. (6)), given by:

$$\underline{V}_G = \frac{1}{2} \frac{m v_{\perp}^2}{q B^2} \underline{B} \times \nabla_{\perp} B \quad (12)$$

under the condition that:

$$\rho_c \frac{\nabla_{\perp} B}{B} \ll 1 . \quad (13)$$

This condition may also be written as

$$V_G \ll v_{\perp} . \quad (14)$$

The gradient drift is therefore a first order drift.

There is a further first order drift, due to the curvature of the magnetic field lines. The radius of curvature of the field line is given by

$$R_C = \frac{B}{\nabla_{\perp} B} \quad . \quad (15)$$

Assuming in the first approximation that the guiding centre follows the curved field line subject to the condition $R_C \gg \rho_c$, we find that the GCS will be a non-inertial system; any mass m in it will thus experience an inertial (centrifugal) force:

$$\underline{F}_C = \frac{mv_{\parallel}^2}{R_C} \hat{n} \quad (16)$$

where \hat{n} is the unit normal directed along the radius of curvature of the field line. This force also causes a drift, given by:

$$\underline{V}_C = \frac{mv_{\parallel}^2}{qR_C B} \hat{n} \times \underline{B} \quad . \quad (17)$$

Since, for a curl-free field,

$$\nabla_{\perp} B = - \frac{B}{R_C} \hat{n} \quad (18)$$

the curvature drift can be rewritten:

$$\underline{V}_C = \frac{mv_{\parallel}^2}{qB^3} \underline{B} \times \nabla_{\perp} B \quad . \quad (19)$$

Since both the curvature drift and the gradient drift are in the same direction and always appear together, we can write the total first order drift as:

$$\underline{V}_{CG} = \frac{m}{2qB^3} (v_{\perp}^2 + 2v_{||}^2) \underline{B} \times \underline{\nabla}_{\perp} B \quad . \quad (20)$$

If the zeroth or first order drifts are time dependent, second order drifts also appear. In this case, a frame of reference which moves with a zero or first order drift \underline{v} will be accelerated, and an inertial force $-m\dot{\underline{v}}$ is observed in that reference frame. Hence, the GCS must move with a velocity \underline{V} plus an additional drift velocity generated by the inertial force, given by:

$$\underline{V}_S = - \frac{m}{qB^2} \underline{v} \times \underline{B} \quad . \quad (21)$$

For the guiding centre approximation to remain valid, the condition:

$$\frac{\tau_c}{V} \dot{V} \ll 1 \quad (22)$$

must be satisfied, where τ_c is the cyclotron period of the particle.

The general expression for the drift velocity of a particle in a non-uniform magnetic field, under the influence of an external non-magnetic force, can be

obtained by combining the zeroth, first, and second order drifts, to be

$$\underline{V}_D = \frac{\underline{B}}{qB^2} \times \left[-\underline{F} + \frac{m}{2B} (v_{\perp}^2 + 2v_{\parallel}^2) \underline{\nabla}_{\perp} B + m\dot{\underline{V}}_D \right]. \quad (23)$$

1.3 The Magnetospheric Substorm

The auroral substorm is part of a magnetospheric substorm (Akasofu, 1968). A magnetospheric substorm usually begins when a southward component of the interplanetary magnetic field causes magnetic field merging on the dayside magnetosphere. Some of the magnetic flux resulting from the merging is transported by the solar wind to the magnetotail. During the transfer process, polarization of the magnetospheric plasma produces an electric field in the magnetosphere. The effect of this electric field mapped into the ionosphere is to generate ionospheric electric currents; in particular, it generates the auroral electrojet, a concentrated electric current induced along a section of the auroral oval. The magnetic disturbance generated by the auroral electrojet and the motions of the protons in the magnetosphere constitute the polar magnetic substorm, which occurs in conjunction with the auroral substorm.

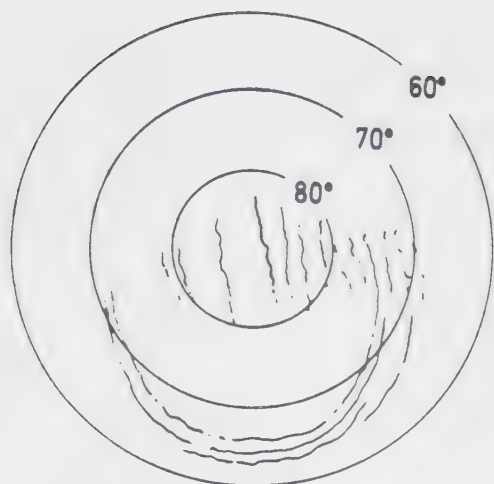
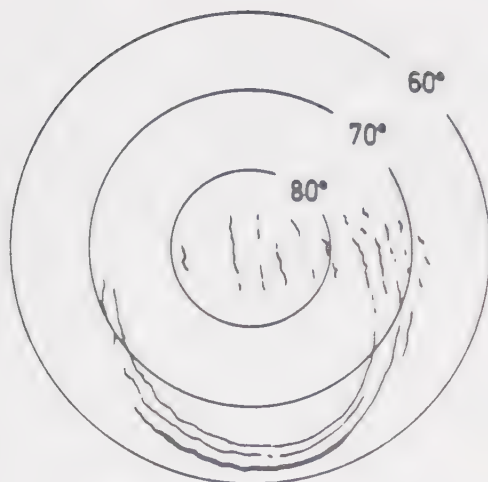
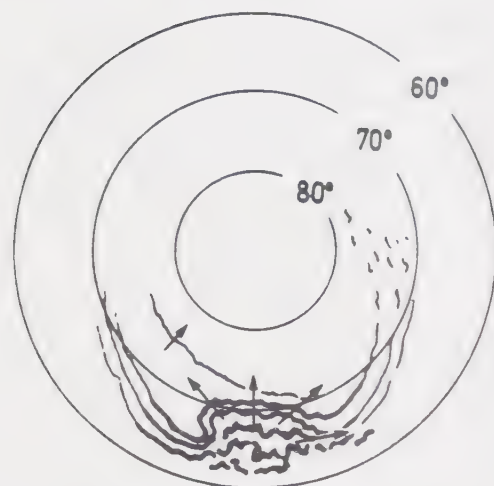
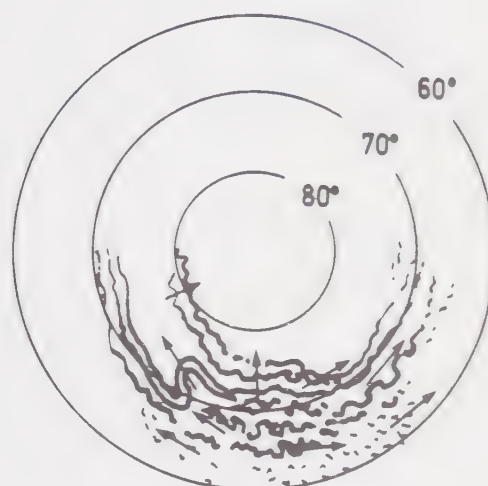
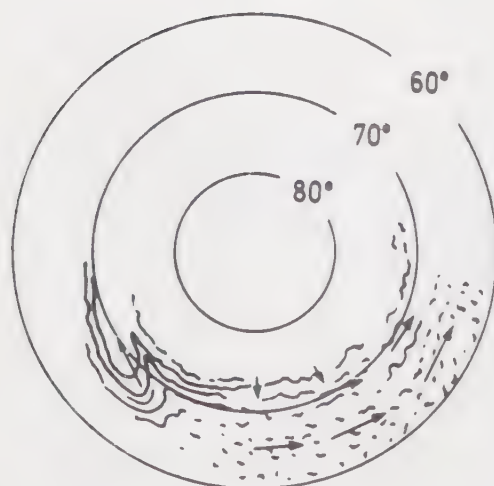
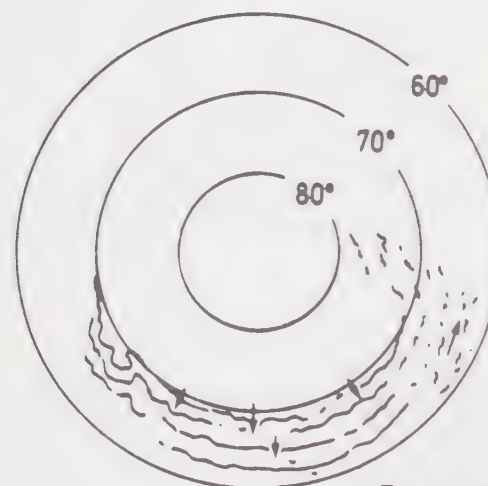
The auroral substorm is defined (Akasofu, 1964) as the sequence of events starting with quiet auroral

conditions, through various phases of activity, to a reversion to quiet conditions.

The seven stages of the auroral substorm can be broadly classified into three phases. During the quiet phase, quiet, homogeneous arcs are present in the midnight sector of the auroral zone. Next is the expansive phase, in which one of the arcs, usually the one farthest equatorward, suddenly brightens. The sudden brightening is usually followed by rapid poleward expansion, resulting in the formation of a bulge around midnight which rapidly expands poleward, westward, and eastward. This process continues until the front of the expanding bulge reaches its most poleward position at which time a westward surge may be seen to develop and move towards the evening sector. This marks the end of the expansive phase. During the recovery phase, the intensity of the arcs diminishes and they begin to drift equatorward, over a wide range of latitude and longitude, until quiet-time conditions are again established. During the initial part of the recovery phase weak loops and folds in the arc structure are seen at the poleward edge of the activated auroral region. The various stages described above are summarized in Figure 1.2.

1.4 Purpose of Thesis

The convection process occurring in the magnetosphere can be considered as a first approximation to be

A $T = 0$ B $T = 0-5\text{min}$ C $T = 5-10\text{min}$ D $T = 10-30\text{min}$ E $T = 30\text{min}-1\text{hr}$ F $T = 1-2\text{hr}$
F \rightarrow A

$T = 2-3\text{hr}$
F \rightarrow A

Figure 1.2

described by steady-state convection, that is, $\partial \underline{B} / \partial t = 0$. Hence, the second order drifts in equation (23) can be neglected. The zeroth and first order drifts of particles in the presence of the enhanced dawn-to-dusk electric field, which causes the growth of the asymmetric ring current during a magnetospheric substorm, are shown in Figure 1.3. We see that the zeroth order drift is directed towards the Earth, while the first order drift is in the azimuthal direction. Hence, the velocity of inward convective drift of the charged particles is given by the zeroth order drift, viz:

$$\underline{V}_D = \frac{\underline{E} \times \underline{B}}{B^2} \quad . \quad (24)$$

The magnitude of the electric field can thus be calculated by obtaining the inward drift velocity of the particles, and using the relation

$$E \cong V_D B \quad . \quad (25)$$

One of the purposes of this thesis is to obtain values of the ionospheric electric fields during periods of auroral activity in the manner described above.

An important contribution will be made from the study of the phase of the associated magnetic substorm during which the auroral arcs were observed. The growth phase of a magnetic substorm (McPherron, 1970) may or may not be accompanied by the presence of equatorward

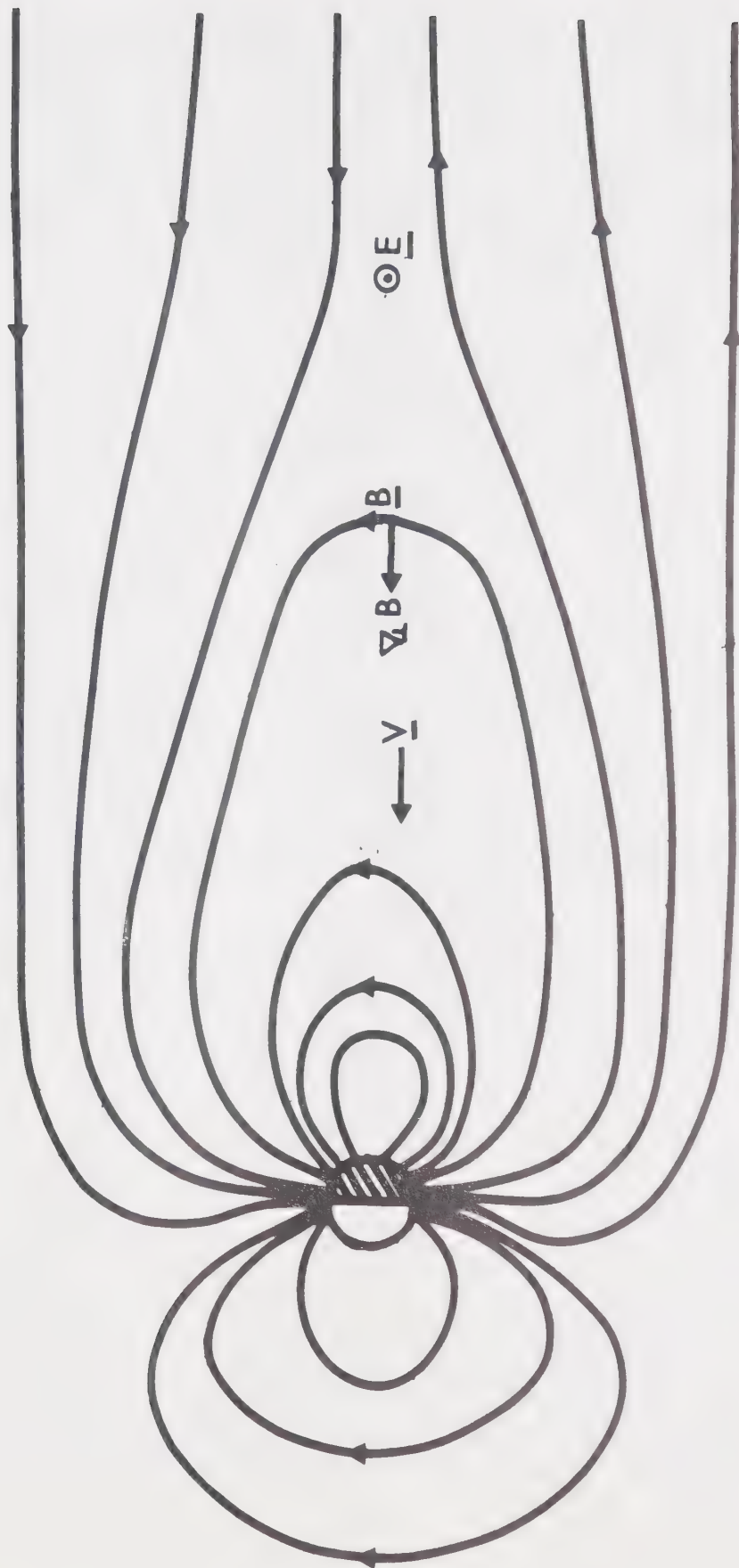


Figure 1.3

drifting arcs, as claimed by Mozer (1971) and Feldstein (1972), however such drifts definitely occur during the recovery phase of the magnetic substorm (Akasofu, 1964). The problem then arises as to whether an observation of equatorward drifting arcs indicates the presence of a growth phase or a recovery phase. This ambiguity will be discussed during the course of this investigation and an explanation is put forward, using a modified version of a theory of the generation of equatorward drifting auroral arcs proposed by Atkinson (1970). This theory is based on the theory of resonant wave-particle interactions (Kennel and Petschek, 1966). Such a mechanism has been used to explain the production of SAR arcs (Cornwall et al, 1971) and the precipitation of Van Allen drift particles in the morning hours (Brice and Lucas, 1971).

2. DETAILS OF THE ANALYSIS

2.1 The All-sky Camera

We have established (eq. 25) that the relationship between the convective drift velocity of particles, V_D , and the associated magnetospheric electric field in the equatorial plane is given by:

$$E \approx V_D B$$

where B is the strength of the ambient magnetic field in the equatorial plane.

This same relationship also holds in the ionosphere, where the quantities involved are the equatorward drift velocity of the magnetic flux tube, the ambient magnetic field in the auroral ionosphere, and the associated ionospheric electric field. The details of the mapping of auroral drift velocities in the ionosphere to convective drift velocities in the equatorial plane, are discussed in the next section.

The drift velocity of the auroral arcs was calculated using all-sky camera (ASCA) photographs from a station at Fort Smith, N.W.T. (68.1°N corr. geomag.). ASCA photographs covering intervals during 1970 and 1971 were studied, over a total sample size of fifteen months. The film data consisted of eight second exposures taken

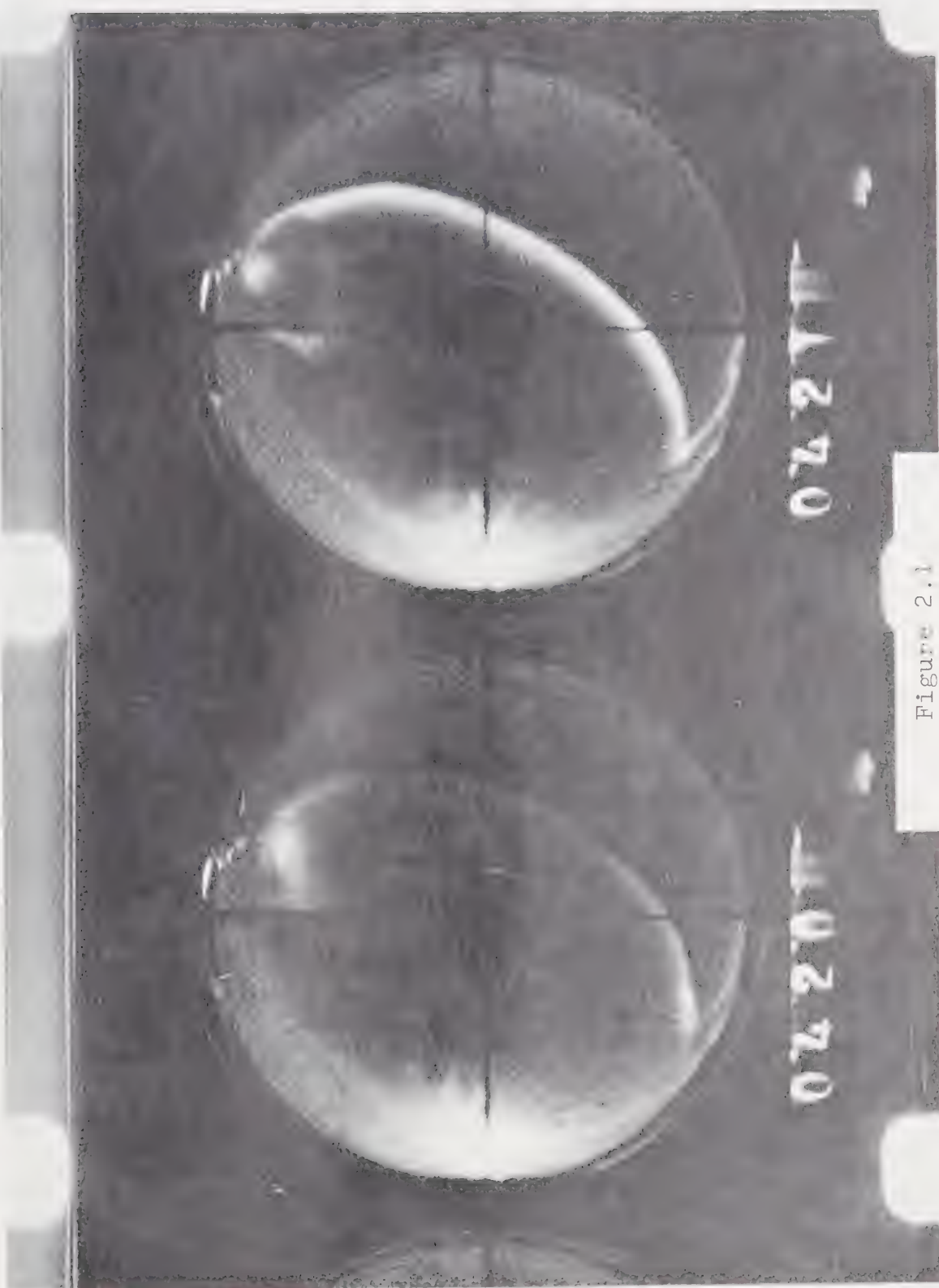


Figure 2.1

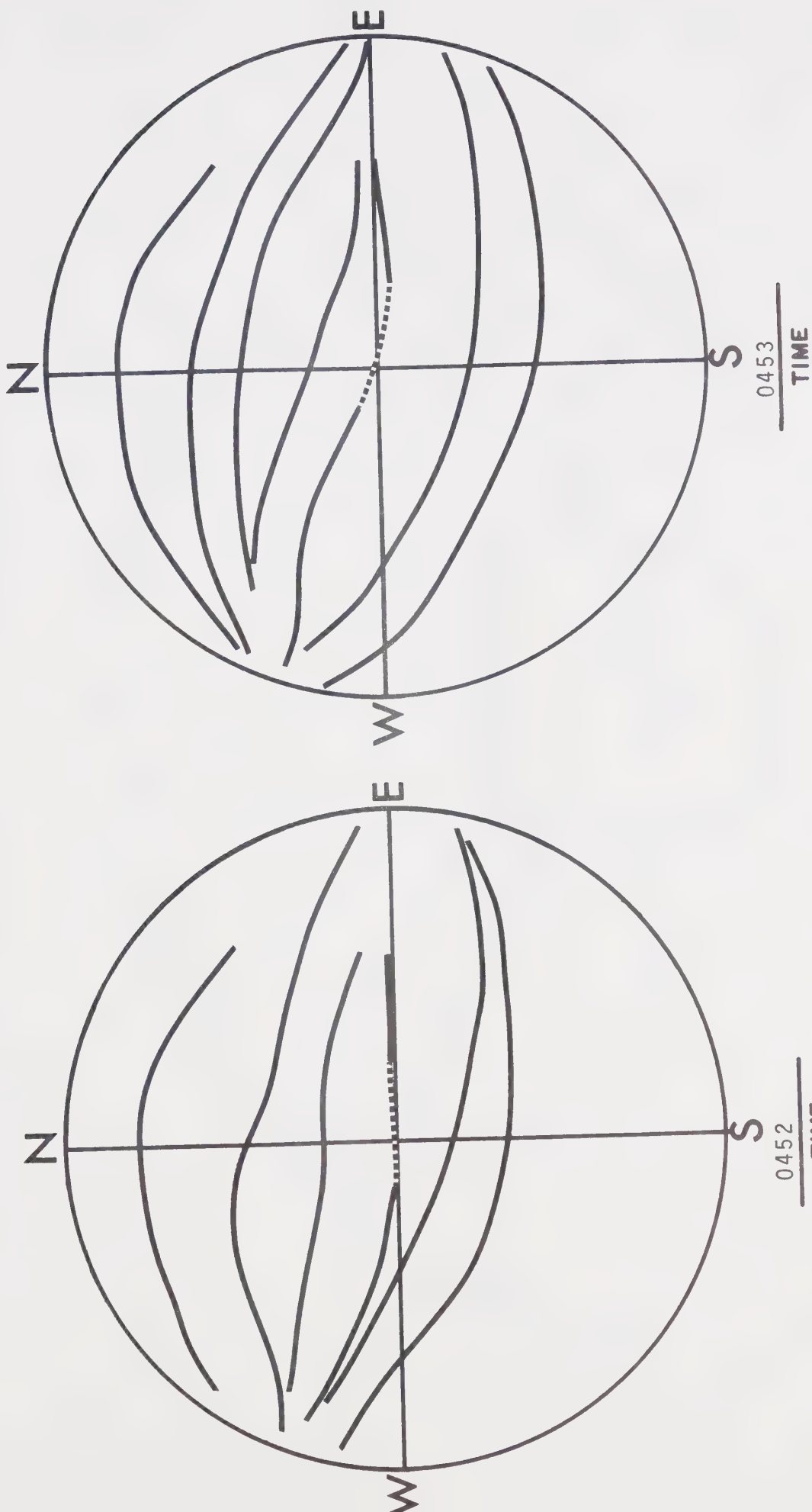
at one minute intervals, at a setting of f 0.95 and using Kodak Tri-X reversal black and white film. A typical ASCA photograph illustrating the form of the data is shown in Figure 2.1.

The eight-second exposure time has an integrating effect on the position of the arcs - that is, motion of an arc during the exposure time is undetected by the camera. To overcome this hurdle, only the motion of the northern or southern boundary of the arc form was followed in successive frames. In addition, the one-minute interval between exposures creates an ambiguity regarding the drift motion of the arcs. We are faced with the question of whether the apparent southward drift of an arc is an actual motion, or the result of the decay of one arc and the establishment of a second arc at a new, more southern position. There is no absolute method of resolving this ambiguity, but it can be reduced to a minimal level by adopting certain criteria in the selection of events for study. The primary criterion was that only those arcs which could definitely be identified as being in motion for a minimum of three frames (i.e. three minutes) were chosen for analysis.

One side effect of the three minute criterion is that many events of short duration were ignored. This fact, together with the possibility that arcs may have

appeared whose brightness was below the threshold sensitivity of the film, had the cumulative effect of reducing the total number of events treated. In all, forty-three cases of southward drift of auroral arcs were identified over the sample interval. We feel that the reasons given above adequately explain the low number of events, in comparison with the number of southward drifting events noted by other workers (e.g. Davis, 1962).

For the purpose of analysis, the arcs were first traced from the film onto ASCA analysis sheets (see Figure 2.2), and then mapped onto a linear scale to eliminate the curvature effect provided by the primary mirror of the ASCA. The mapping was done by means of an auroral arc mapper. The mapper is a template (see Figure 2.3), on which holes are drilled at closely spaced points along two curved loci. Each of the holes on the two loci is connected to a point on the inside edge of the template by a straight line, as shown in the figure. Each of the edge points connected to the holes is superposed in turn on the auroral arc positions on the tracing, and the hole position is marked. The position of the hole corresponds to arc position on a linear scale. The mapped points are then joined to obtain the form of the mapped auroral arc. The velocity of southward drift was determined from the successive positions of the mapped arcs (Figure 2.4). The technique



OCTOBER 8, 1971

PORT SMITH

CAMERA

Figure 2.2

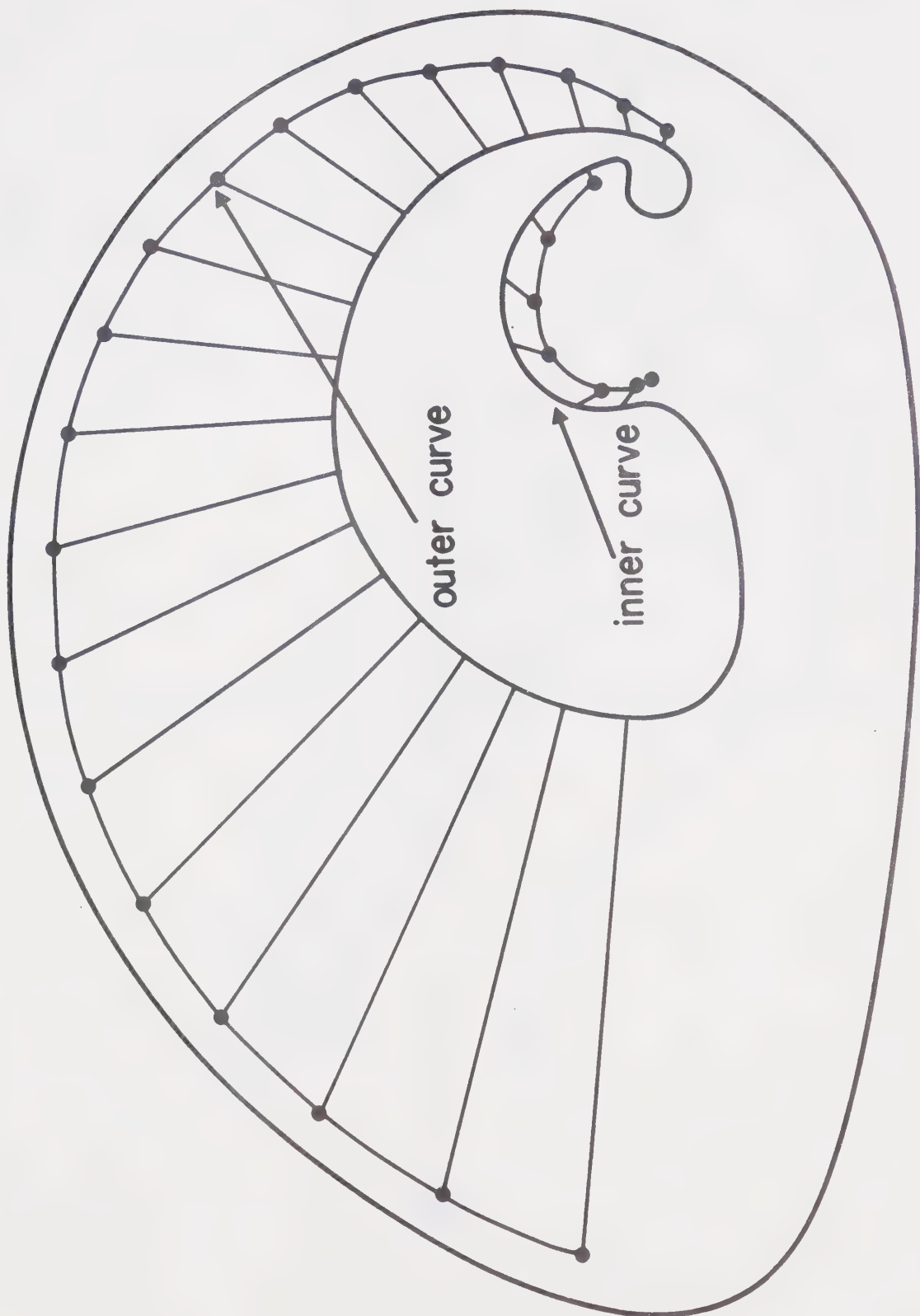


Figure 2.3

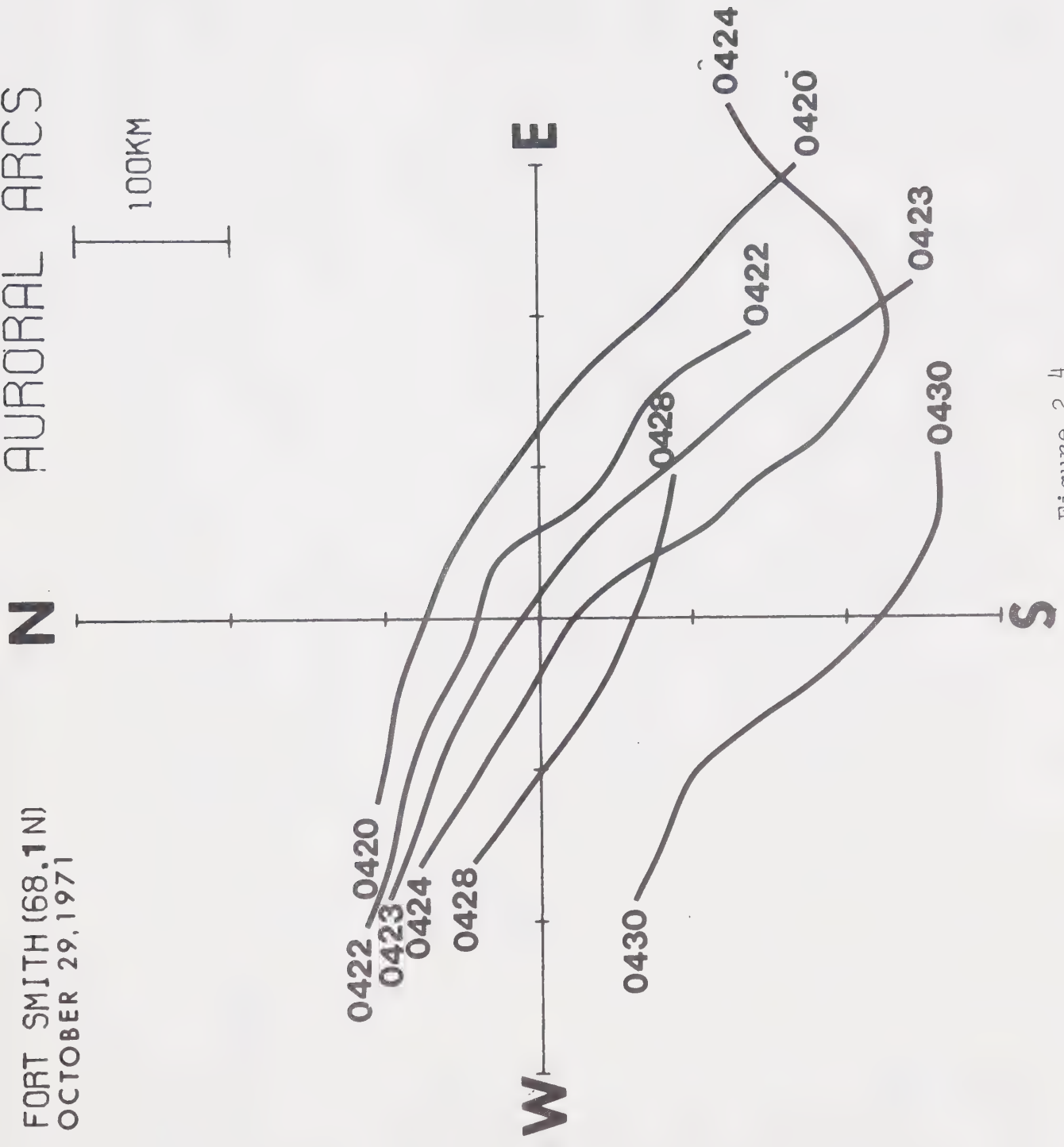


Figure 2.4

of inferring convective motion in the magnetosphere from the drift velocity of auroral arcs has been used previously by several workers (e.g. Davis, 1971; Kelley et al, 1971).

2.2 The Mapping Factor

The velocity obtained from the motion of the mapped arcs is the drift velocity of the arcs in the ionosphere. The value of the electric field that is eventually determined is also the ionospheric value. However, we also wish to compare the value of the electric field in the equatorial plane, as obtained from this method, with the values obtained by other means. It is therefore necessary to have a mapping factor between the ionosphere and the equatorial plane. The velocity thus obtained in the equatorial plane is an indication of the convective drift velocity of particles in that region. The mapping factor has been calculated by Mozer (1970), and is given by the ratio of the westward electric field in the ionosphere to that in the equatorial plane.

$$\frac{E_{Wi}}{E_{We}} = L^{3/2} .$$

The L value corresponding to Fort Smith is ~7; this gives a value of 18.5 for the mapping factor. The mapping

factor for velocities, then is given by:

$$\frac{V_e}{V_i} = 18.5 \quad .$$

It should be pointed out that this mapping assumes a dipolar magnetic field in the absence of parallel electric fields. Such a situation does not occur often in reality, and the effects of deviations from the ideal ought to be examined. The non-dipolar character of the field lines in the nightside magnetosphere does not alter the basic law of conservation of magnetic flux, which is the underlying principle in the theory of the mapping. It does, however, alter the geometry of the field, and thus the mapping factor from the magnetosphere to the ionosphere is affected. Hence, the final value of the mapping factor may be different from $L^{3/2}$, by some factor depending on the magnitude of the distortion of the field from the dipolar configuration. Even if this were not the case, the change in L value as the arcs move equatorward may contribute a significant error.

If parallel electric fields are present, there will be a potential drop along the field line from the magnetosphere to the ionosphere. If the potential drop is the same along neighbouring field lines, then the expression for the mapping factor still remains valid. This implies that there should not be much longitudinal variation in the electric field.

It is difficult to know quantitatively how well these conditions for validity are met. Because of this difficulty the effect of these errors cannot be accurately incorporated into the calculations done here. However, their presence certainly ought to be recognised.

2.3 Magnetic Data

The magnetic effects associated with the events under analysis were studied to determine the phase of the polar magnetic substorm corresponding to the time of appearance of southward drifting arcs. This question is of some importance since some workers have claimed that southward drifting arcs are associated with the growth or development stage of the associated polar magnetic substorm (Belyakova et al, 1968; Feldstein, 1972; Mozer, 1971). It has also been claimed that the growth phase has a ground-based magnetic signature (McPherron, 1970).

We have therefore approached this problem by examining the ground-based magnetic records associated with our events using all auroral zone stations in the North American sector. A list of these stations and their geomagnetic co-ordinates is given in Table 2.1. To identify the phase of the associated magnetic substorm, a tentative phase was assigned to the substorm at each

Table 2.1

Coordinates of Magnetic Observatories Whose
Records are Used in This Study

Observatory	Geographic		Coordinates	
	(°N)	(°E)	Corr. Geomag. (°N)	(°E)
<u>Used to Determine Phase of Substorm</u>				
Great Whale River	55.3	282.2	68.2	353.8
Fort Churchill	58.8	265.8	70.3	325.9
Baker Lake	64.3	264.0	75.1	320.4
Meanook	54.6	246.7	62.5	301.2
Sitka	57.0	224.7	59.8	276.6
College	64.9	212.2	64.9	260.3

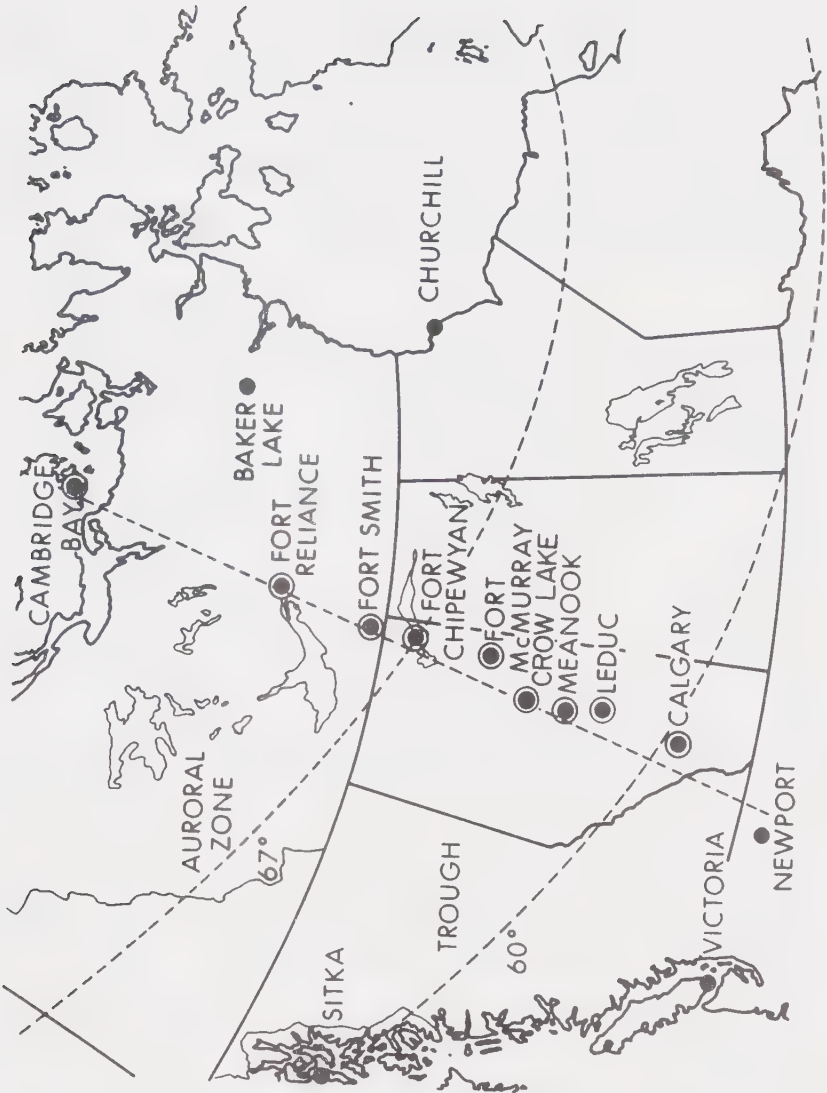


Figure 2.5

station after an independent examination of the station's magnetic records. Then these assigned phases were compared for each event to determine if the results were self-consistent. In cases of ambiguity or inconsistency, the records of the station under question were reexamined, this time in conjunction with the information available from the other stations. It will be seen later that in some cases the ambiguity remained unresolved even after the reexamination.

In addition, the behaviour of the associated current systems was also determined, through a study of the corresponding latitude profiles for each event. (See Kisabeth and Rostoker (1971) for details of latitude profiles.) The latitude profiles were obtained using the magnetic data from the University of Alberta line of magnetometer stations in Alberta and the Northwest Territories. The stations lie along the corrected geomagnetic meridian of $\sim 301^{\circ}\text{E}$ and are closely spaced in the latitude range 58° to 77°N . Supporting data were obtained from the standard observatories at Newport, Baker Lake, and Resolute Bay at 55.3°N , 75.1°N and 84.3°N respectively. The locations and co-ordinates of these stations are shown in Fig. 2.5 and Table 2.2. A three-component fluxgate magnetometer operated at each of the stations along the line, recording the three components (H,D,Z)

Table 2.2

Coordinates of Magnetic Observatories Whose
Records are Used in This Study

Observatory	Geographic		Coordinates	
	(°N)	(°E)	Corr. Geomag. (°N)	(°E)
<u>Used to Create Latitude Profiles</u>				
Resolute Bay	74.7	265.1	84.3	306.0
Cambridge Bay	69.1	255.0	77.7	301.0
Fort Reliance	62.7	251.0	71.4	300.0
Fort Smith	60.0	248.0	68.1	300.8
Fort Chipewyan	58.8	248.0	67.0	301.6
Fort McMurray	56.7	248.8	65.0	302.7
Meanook	54.6	246.7	62.5	301.2
Leduc	53.3	246.5	61.2	301.5
Calgary	51.2	245.5	58.7	302.0

of the magnetic perturbation field in digital form on magnetic tape. The sample rate was one data point for each component every two seconds, with the timing accurate to ± 0.1 sec. The dynamic range of the system was $\pm 1000\gamma$ with a sensitivity of $\pm 1\gamma$. In the latitude profile, the perturbation components (H,D,Z) are plotted for a given instant of time as a function of geomagnetic latitude of the stations. Successive latitude profiles therefore show the development of the current system in time.

3. PRESENTATION OF THE DATA

3.1 Observational Results

The electric field values obtained from the forty-three cases of southward drifting arcs which were identified are summarized in Table 3.1. A detailed table showing the parameters evaluated for each event appears in the Appendix.

The values of the ionospheric electric field obtained here compare favorably with the ionospheric electric field measurements in the auroral zone obtained by different methods, such as balloon borne electric field probes (Mozer and Manka, 1971) and barium cloud techniques (Haerendel and Lüst, 1970). The average value of 16 mV/m for the ionospheric electric field corresponds approximately to a westward directed magnetospheric electric field of ~ 0.9 mV/m in the equatorial plane at $L \approx 7$. This is nearly an order of magnitude greater than the values obtained through whistler techniques (Carpenter et al, 1972); however, their whistler measurements were made at L values corresponding to locations inside the plasmasphere. The fact that the ring current may shield the plasmasphere from the electric fields outside the plasmopause (Vasyliunas, 1971; Chen and Wolf, 1972) mitigates this discrepancy to a large extent. Some error is also introduced from the effect of the Earth's

Table 3.1

Electric Field Values Inferred From Southward
Drifting Arcs

Minimum Value	5 mV/m
Maximum Value	37 mV/m
Average Value	16 mV/m
Standard Deviation	± 7 mV/m

Table 3.2

Summary of Magnetic Correlation

Number of southward drifting arcs in sample	43
<u>Magnetic signatures during event:</u>	
No activity	1
Recovery phase (in whole or in part)	34
Expansive phase onset (in whole or in part)	7
Not definitely identifiable phase of sub- storm (in whole or in part)	23
Growth phase	0

rotation under the auroral oval during the evening sector (Akasofu et al, 1966). Akasofu and his colleagues have calculated that on the average, the rotation of the Earth under a stationary oval gives rise to an apparent drift velocity of 40-50 m/sec. This would correspond to a magnetospheric electric field value of $\sim 0.08-0.1$ mV/m. Although this is not a large value, it should be noted that this error is present in most of the values of the electric field obtained, since most of our events occurred in the evening sector (see Appendix).

It is interesting to note that the equatorward drift velocity distribution obtained by Akasofu et al (1966) has a peak in the range 100-250 m/sec; a similar distribution for our results shows a peak in the range 400-600 m/sec.

Table 3.2 shows, in summary, the correlation between equatorward drifting arcs and the level of magnetic activity recorded at auroral zone stations, as described in section 2. The term "in whole or in part" which appears in this table is indicative of either cases where different phases appeared to be in progress at the different stations, or cases where it was impossible to definitely identify the phase of the substorm. However, it can be stated that none of the ambiguous cases were associated with a growth phase,

including the 23 cases for which no definite phase could be assigned. In fact all but one case occurred within intervals of clear substorm activity, and as the one case when no substorm was in progress, no substorm activity followed the time when the southward drifting arcs were observed. Hence, none of the 43 events identified was associated with pre-substorm effects (or a growth phase) while the great majority of cases (namely 34 of 43) were associated with the recovery phase of the polar magnetic substorm. We note however that the absence of southward drifting arcs during a growth phase does not imply the absence of an enhanced westward electric field in the ionosphere during the pre-substorm period (Kelley et al, 1971).

The latitude profiles associated with the events, observed on the meridional line of stations, showed well-defined magnetic perturbation, associated with the appearance of southward drifting arcs; however, the magnitudes of these perturbations were not in general large compared with the magnitude of the substorm within which the perturbation occurred. Some sample events are discussed in the next section; the Appendix gives the profiles for selected events.

3.2 Sample Events

We consider first events 20-24, which occurred on October 9, 1971 during the interval 0250-0330 UT. We

note that events 20 and 21, and 22, 23, and 24 involve multiple arcs (see list of events in Appendix). This type of structure is typical of southward drifting arcs (Akasofu et al, 1966). Figure 3.1 shows the latitude profiles near the beginning and end of events 20 and 21. The very large positive ΔH regime and small negative ΔZ regime indicate the presence of both an eastward and westward electrojet. The presence of these two equally strong electrojets is to be expected in the evening sector (Kisabeth, 1972). We note that the boundary between the eastward and westward jets is the site of the arc development ($\sim 68^\circ\text{N}$). As the arcs drift southward, so does the boundary between the two electrojets. This is shown very clearly in Figure 3.2, which shows the profiles near the beginning and end of event 22. The double electrojet system continues to the end of the events, as shown by the arc locations in Figure 3.3 (events 23 and 24). We note also the sudden enhancement in the ΔD profile at Fort Reliance (71.4°N and corr. geomag.), shown by means of a differential profile in Figure 3.4 (corresponding to event 24). A large negative ΔD is indicative of an enhanced convection across the polar cap; such an enhancement is not unreasonable under the circumstances, i.e. during an auroral substorm.

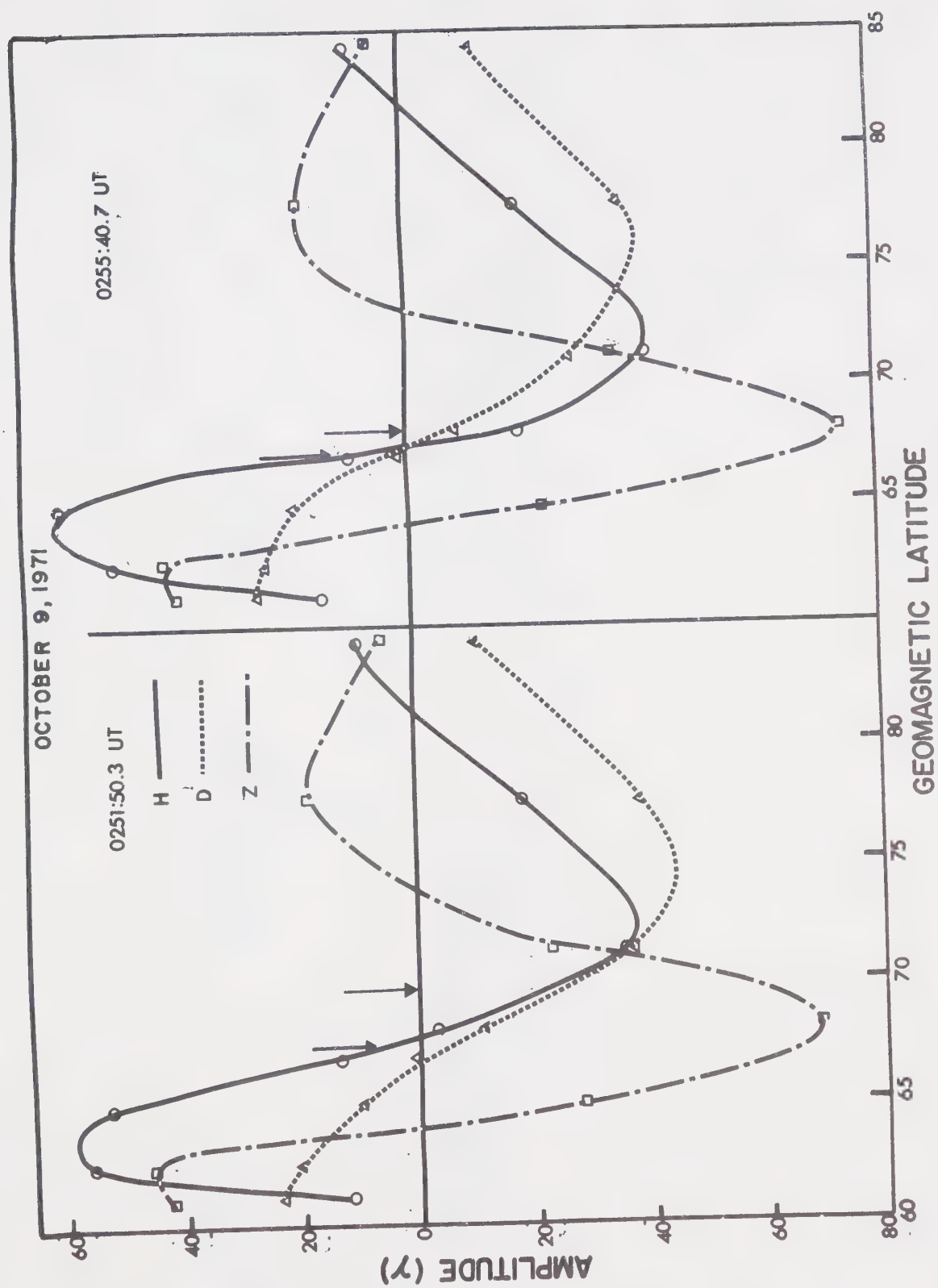


Figure 3.1a

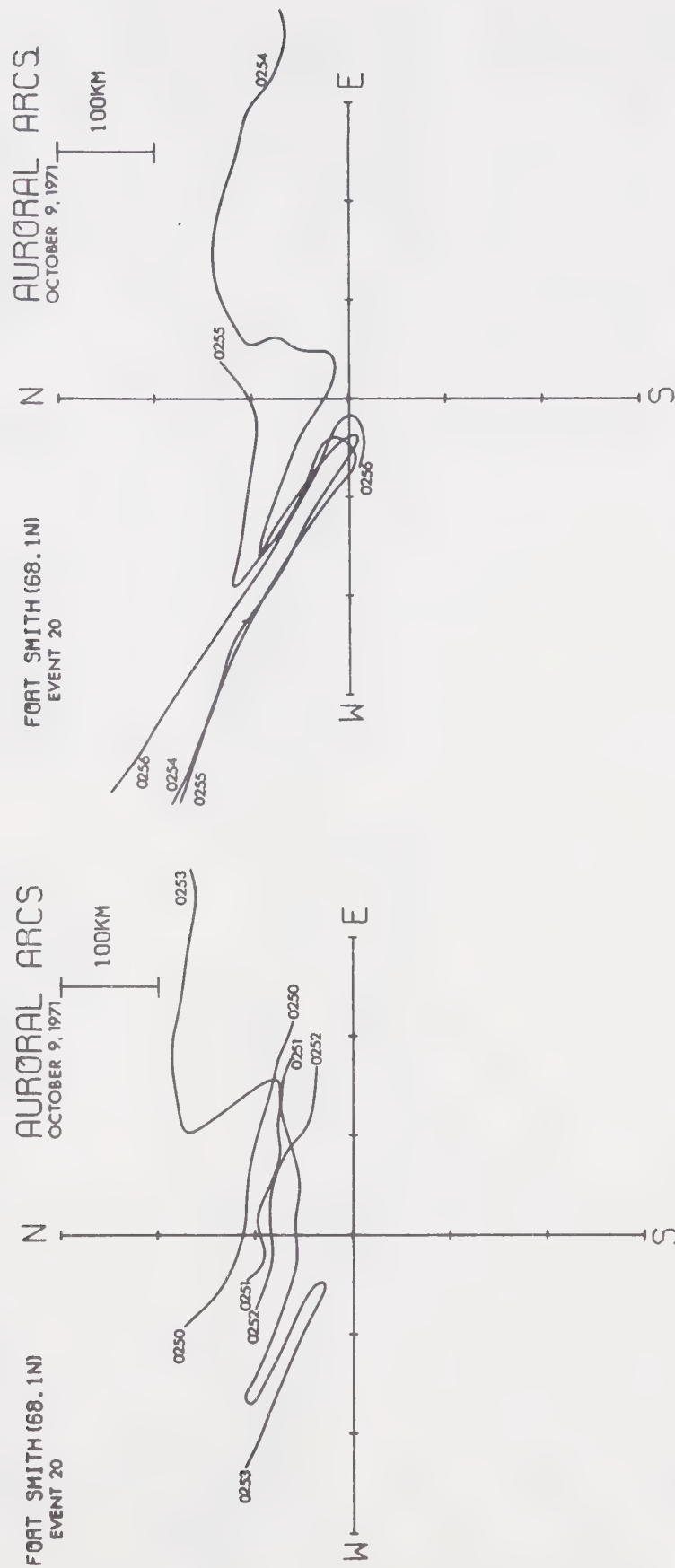


Figure 3.1b

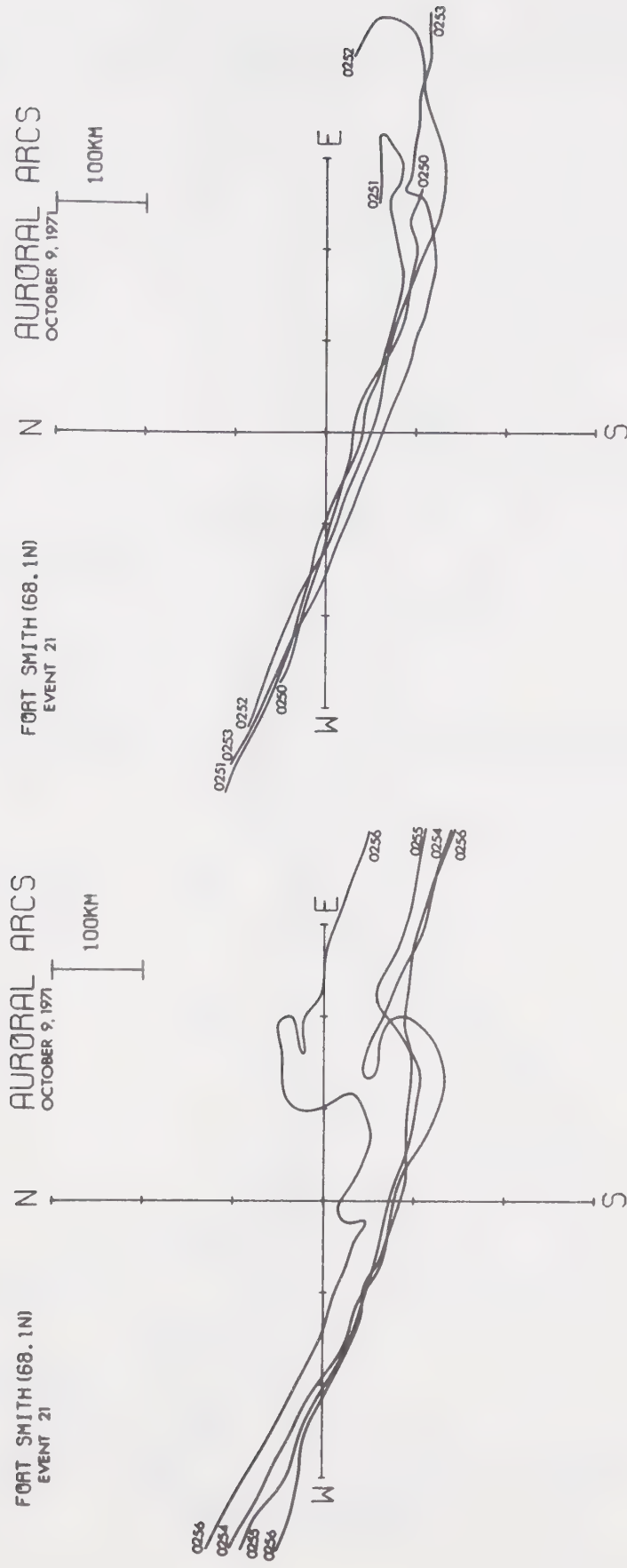


Figure 3.1c

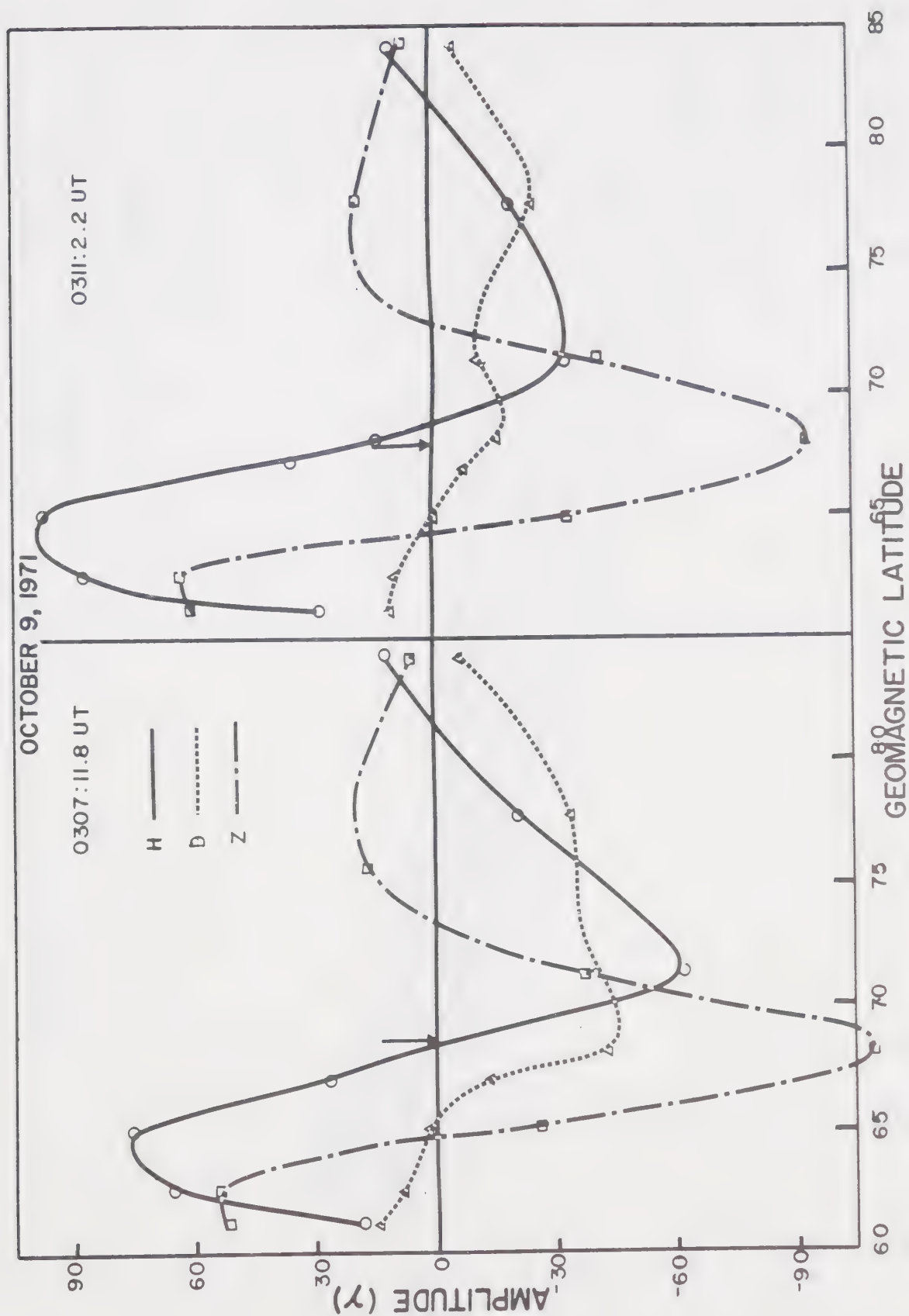


Figure 3.2a

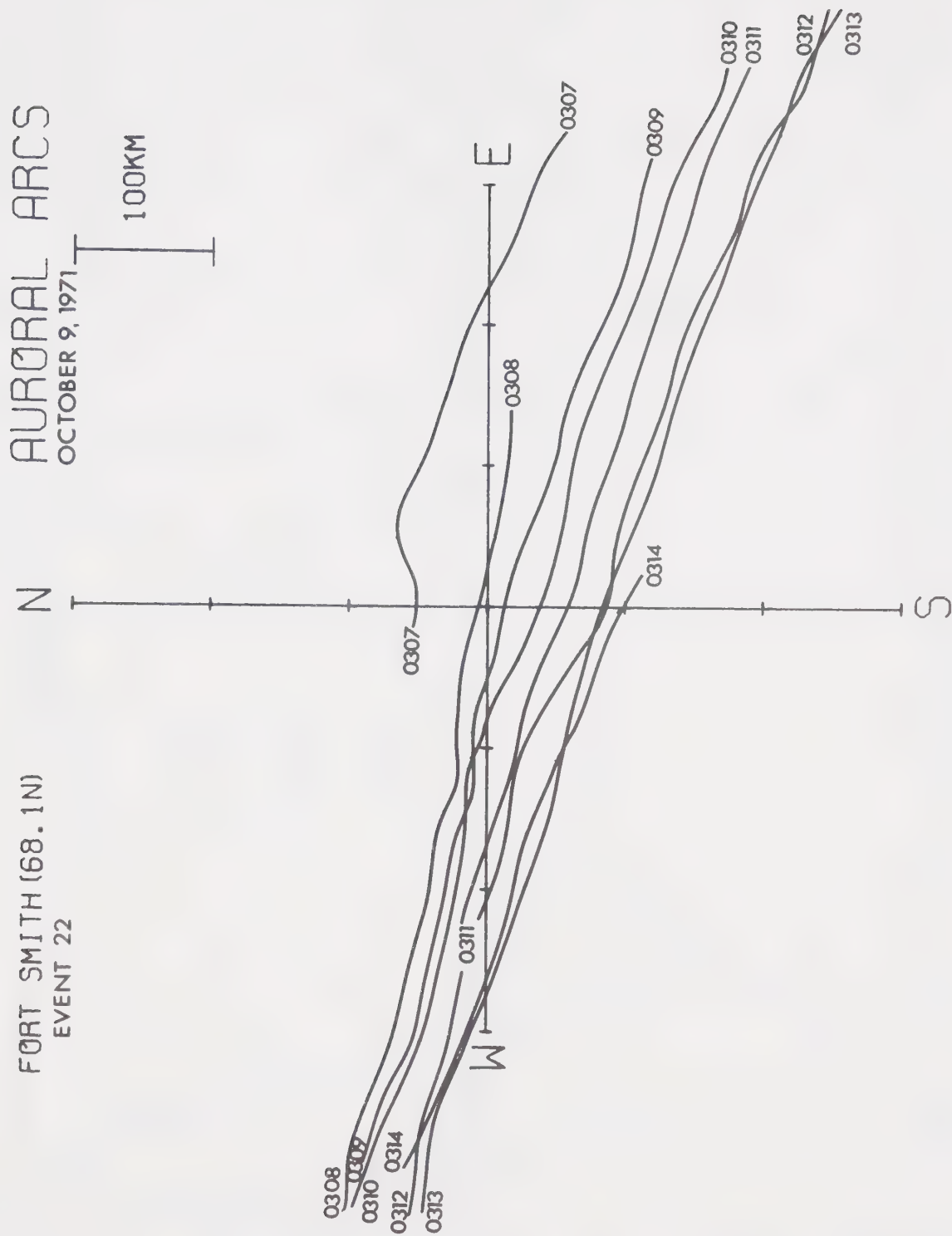


Figure 3.2b

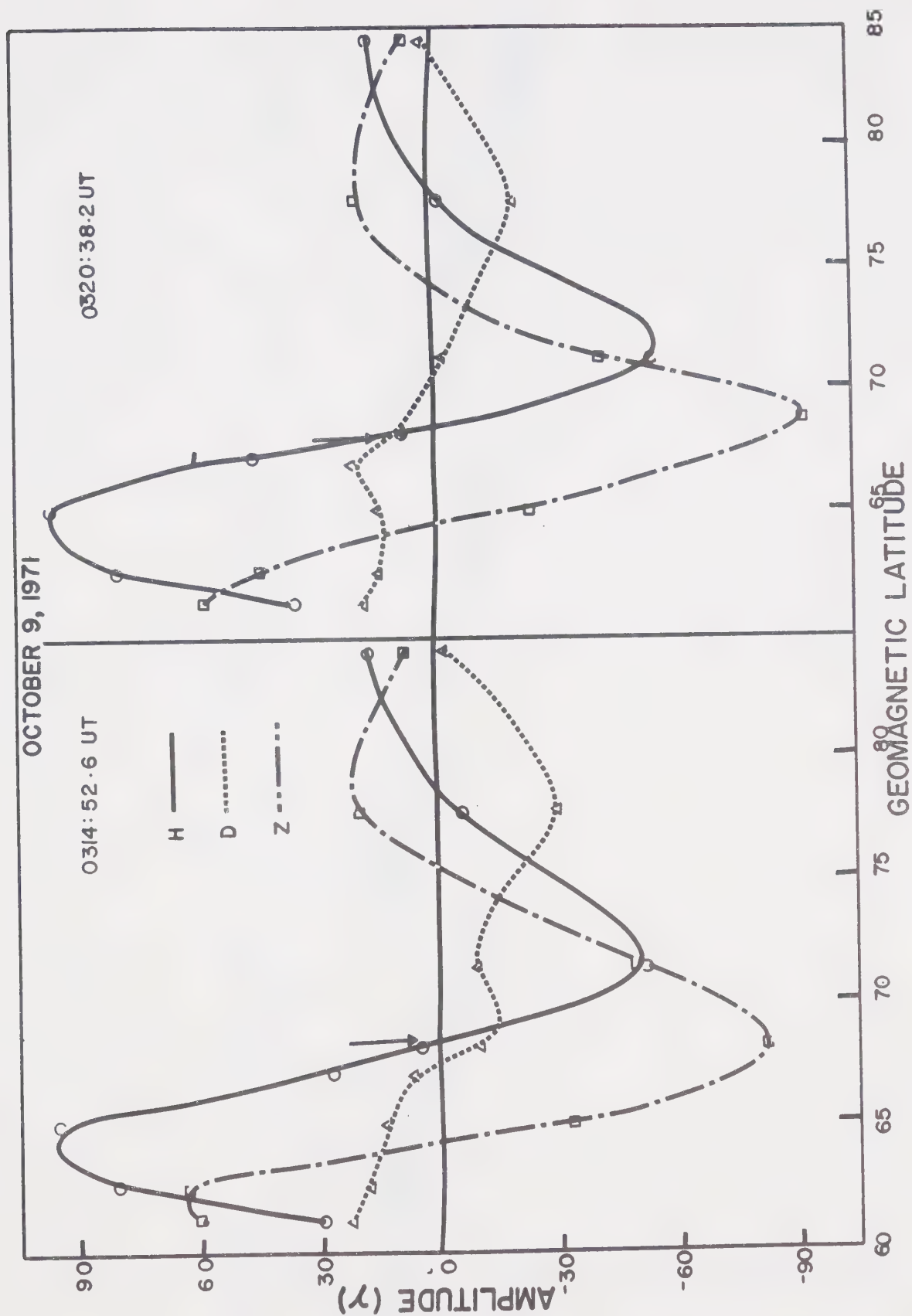


Figure 3.3a

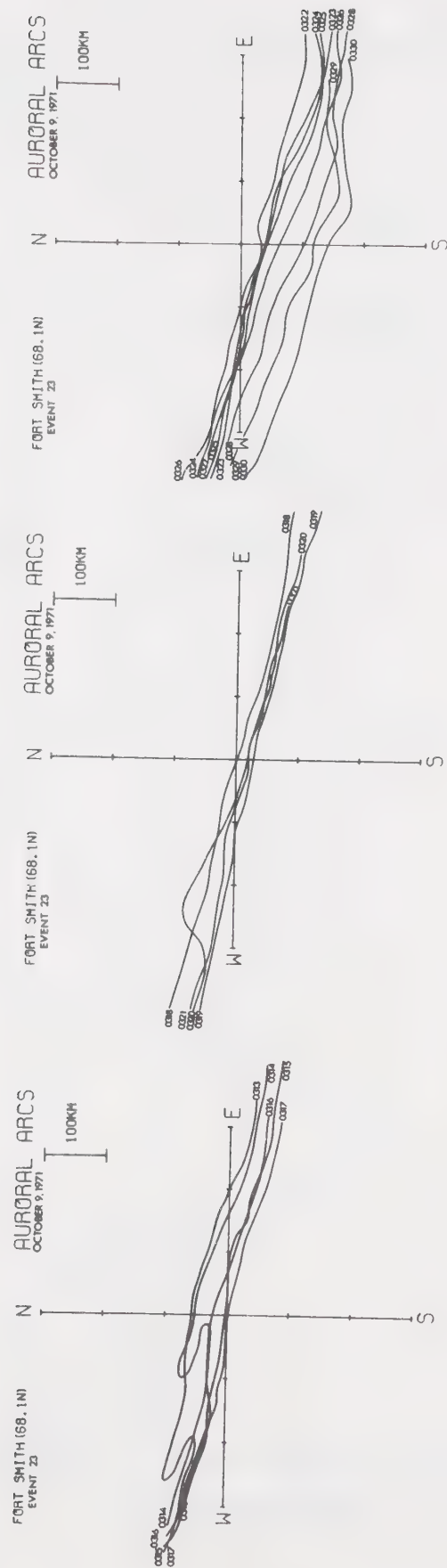


Figure 3.3b

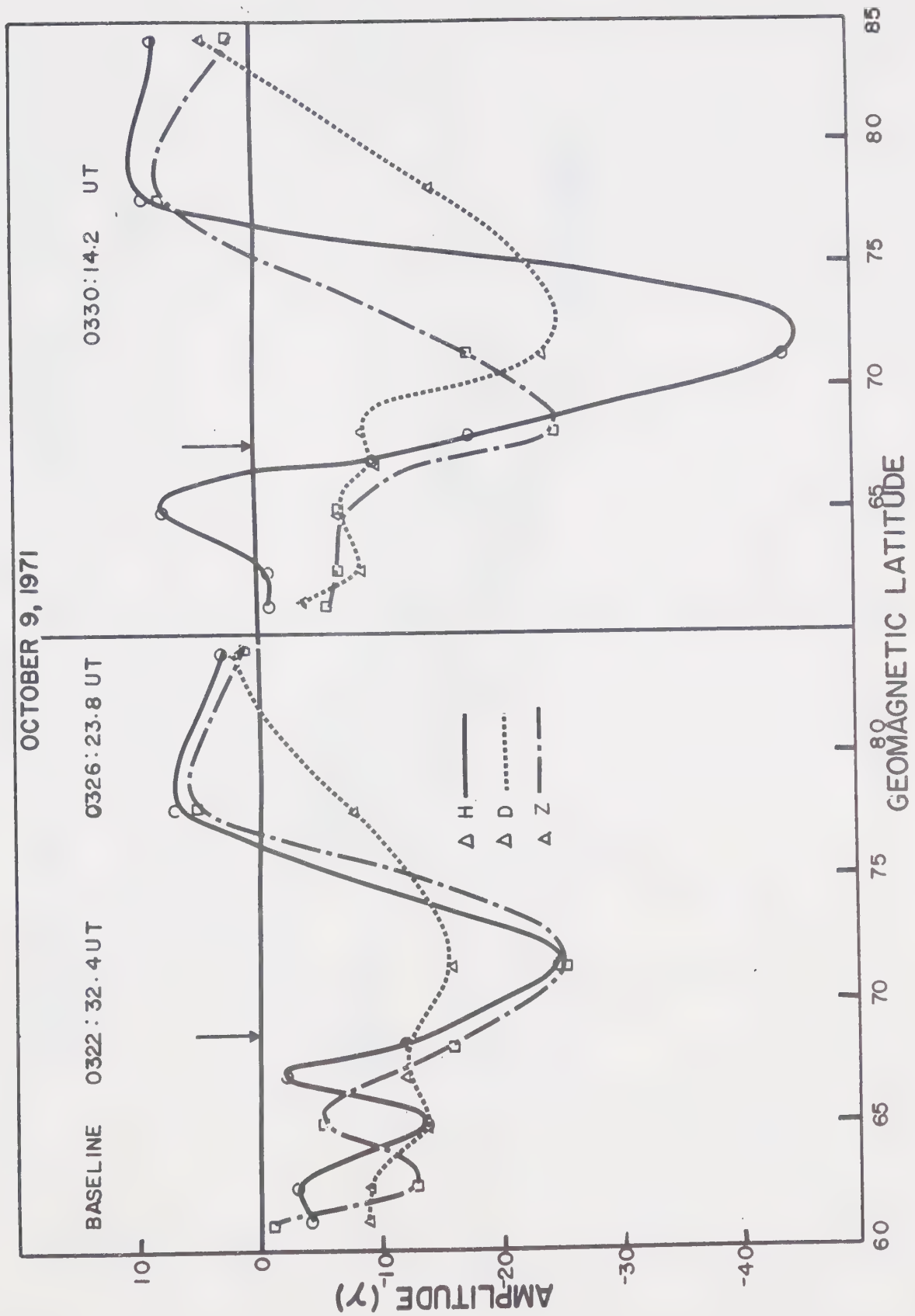


Figure 3.4a

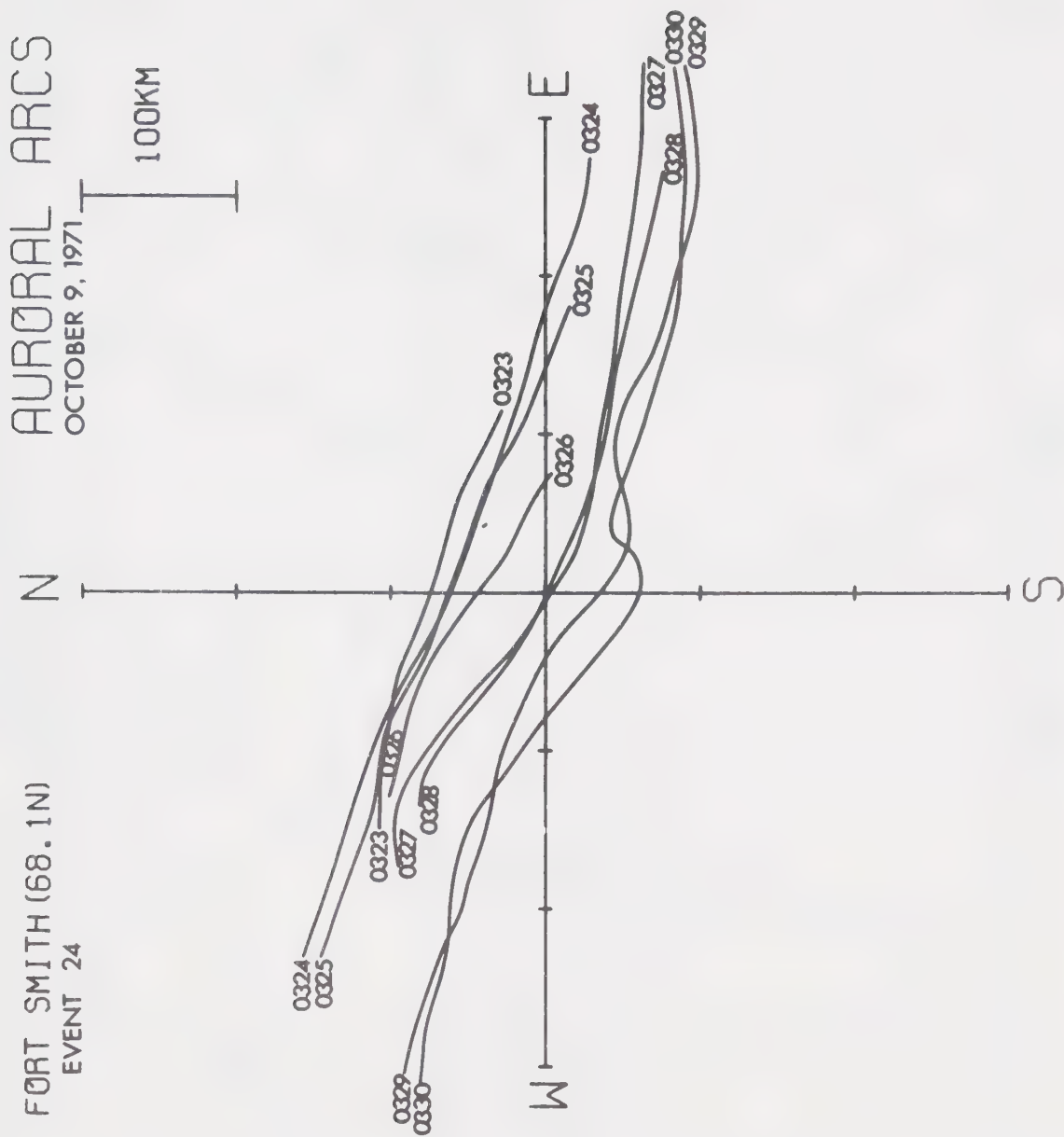


Figure 3.4b

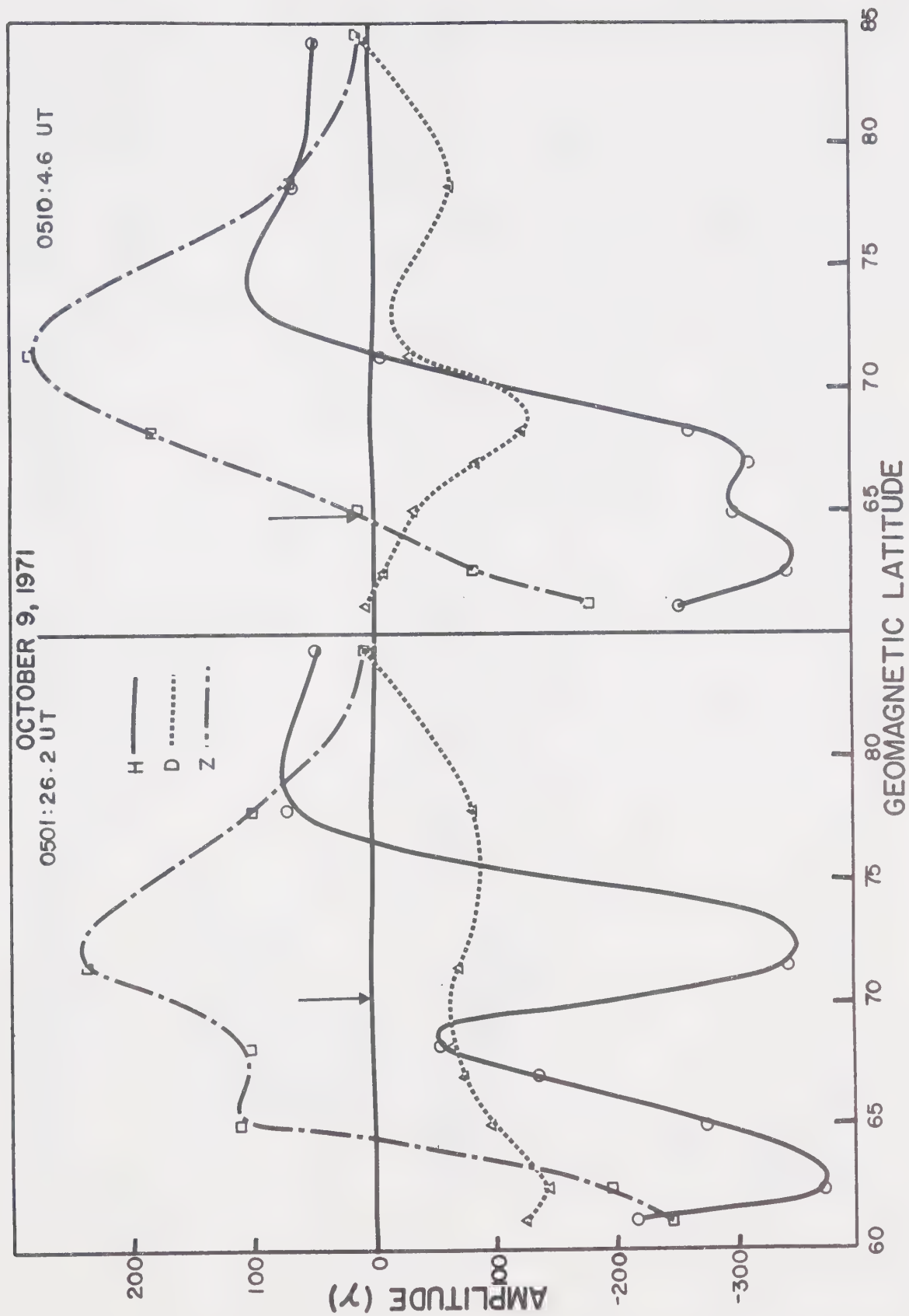


Figure 3.5a

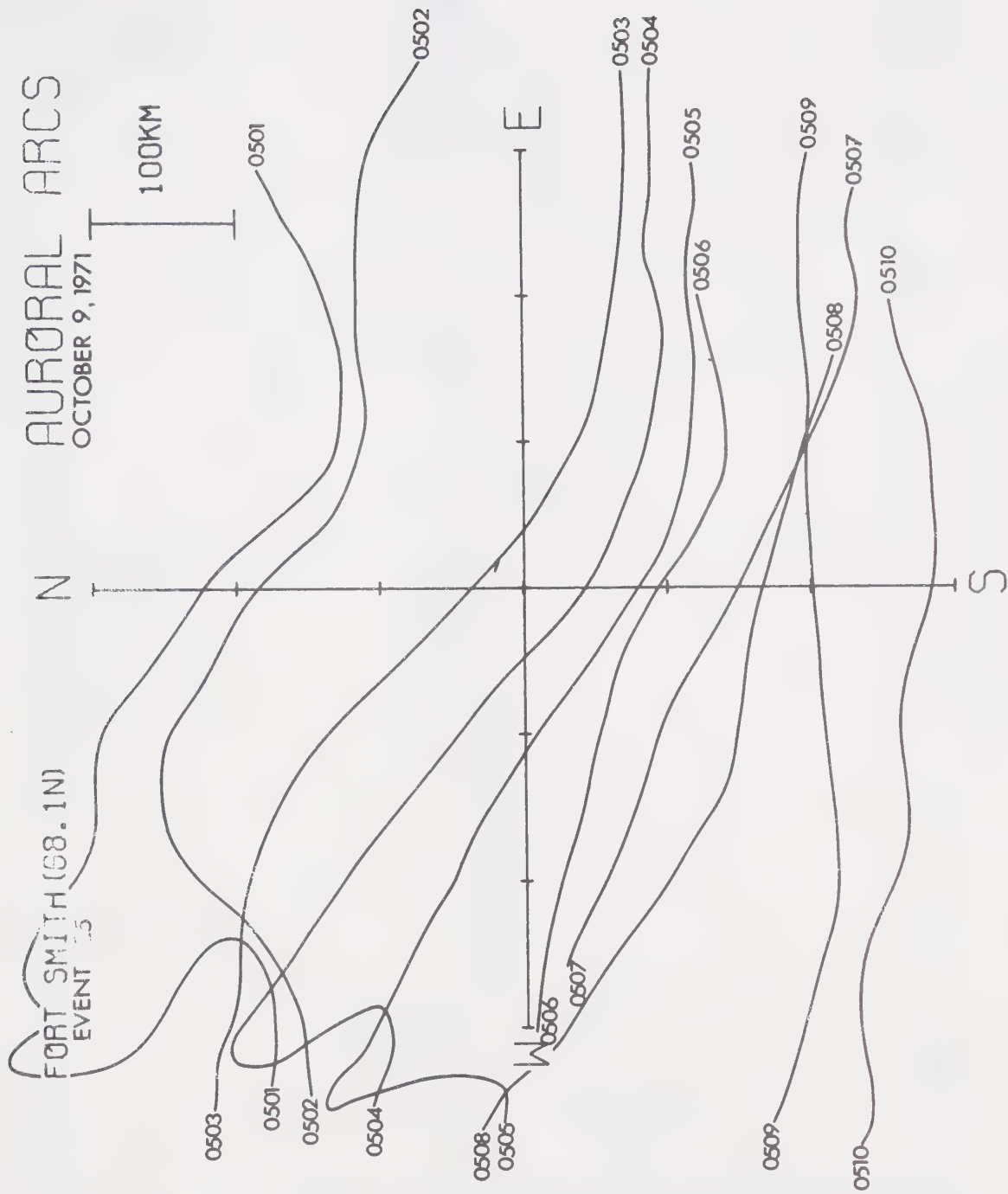


Figure 3.5b

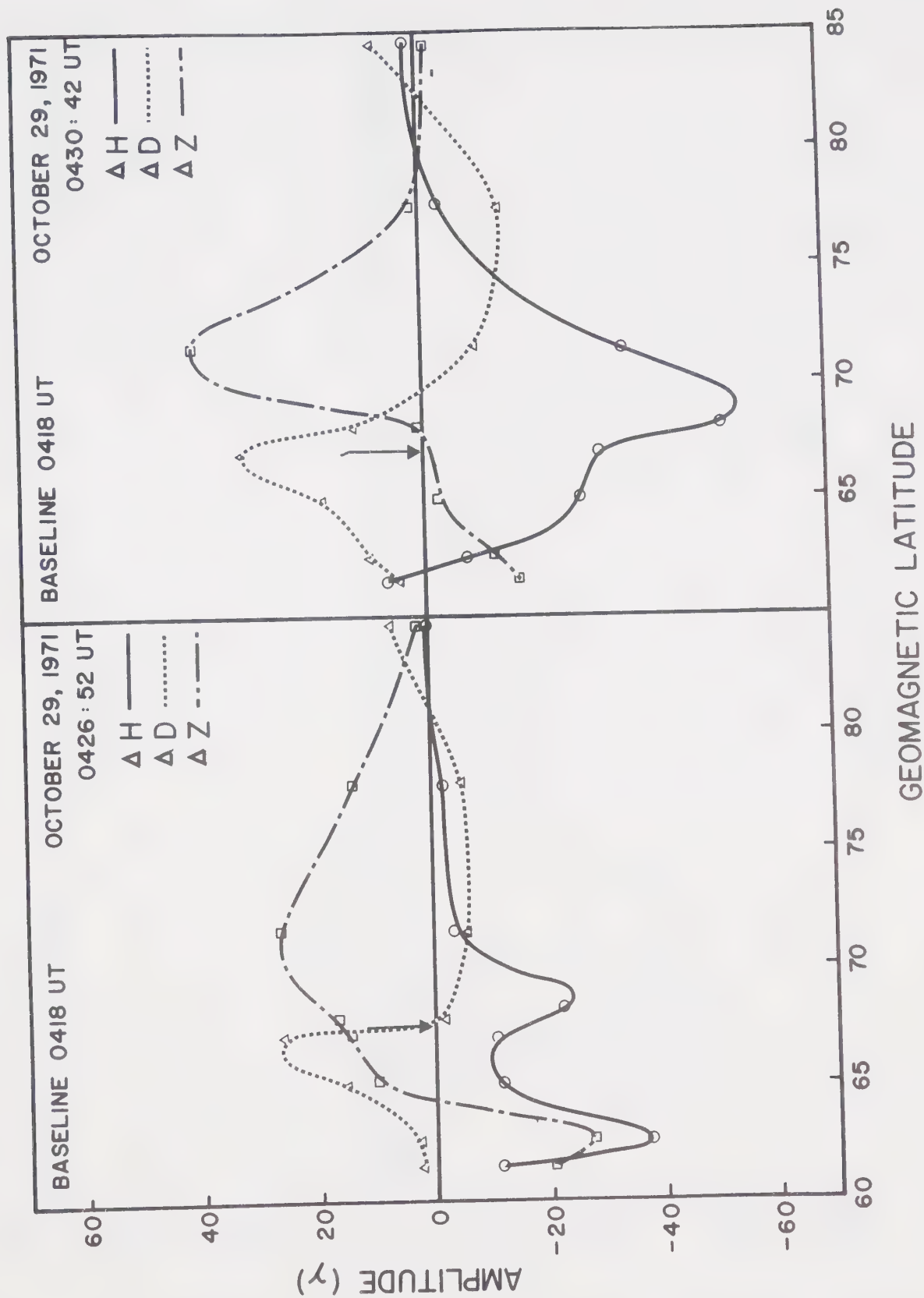


Figure 3.6

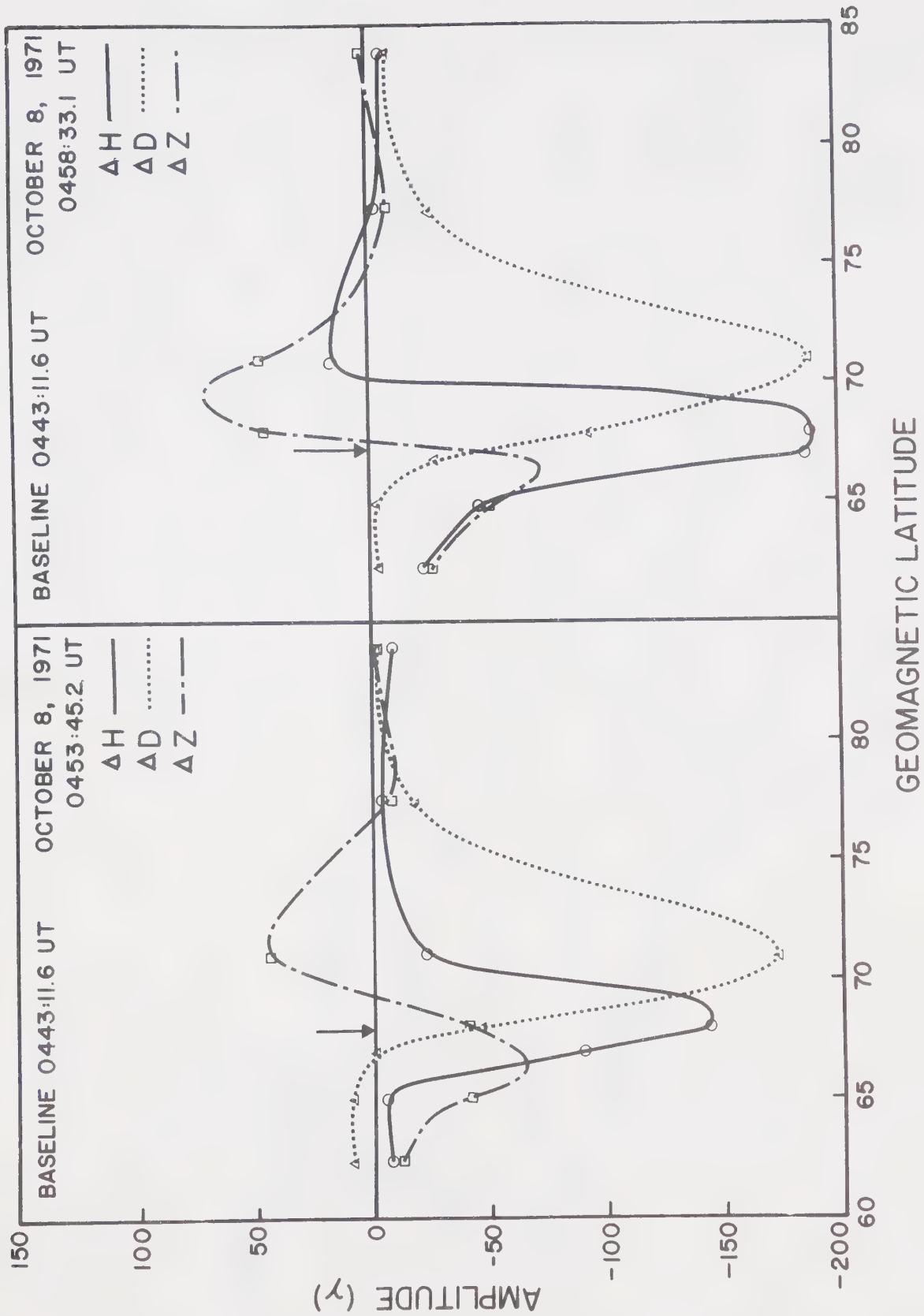


Figure 3.7a

AURORAL ARCS

100KM

N

FORT SMITH (68.1N)

OCTOBER 8, 1971

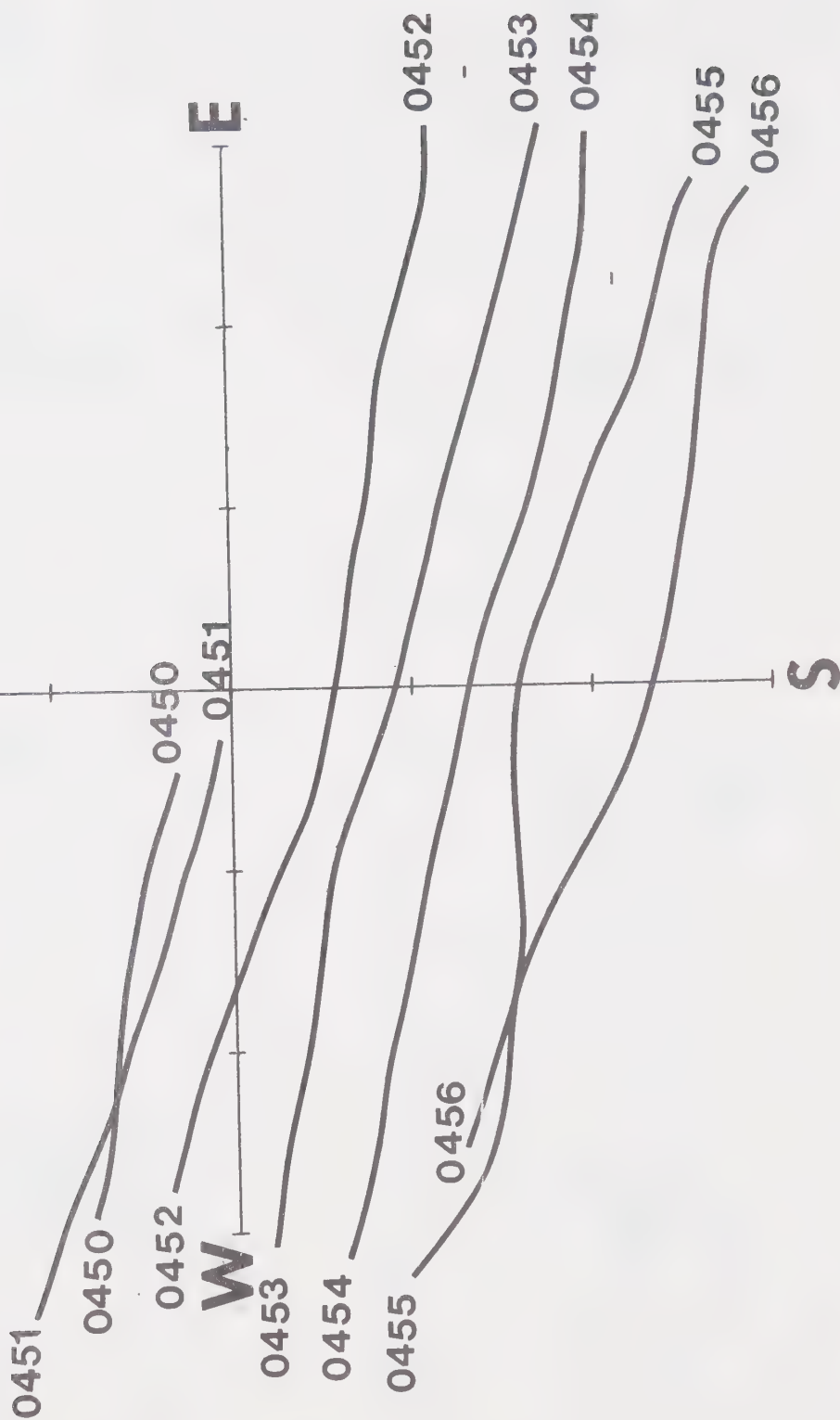


Figure 3.7b

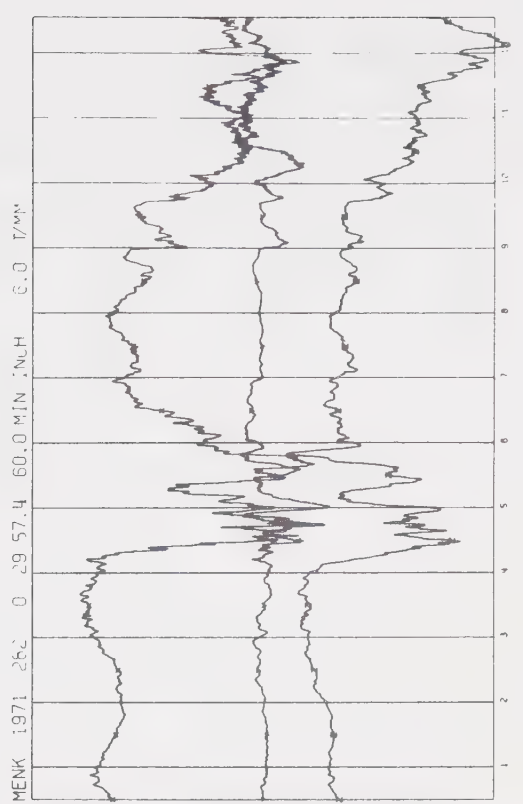
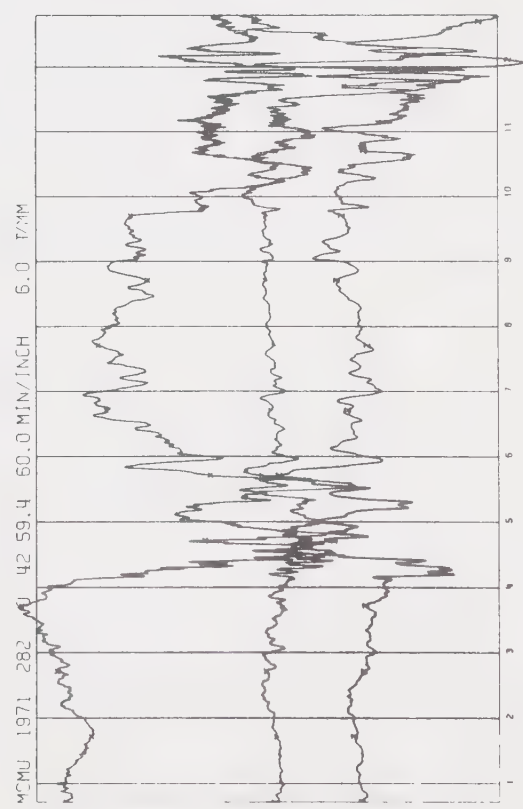
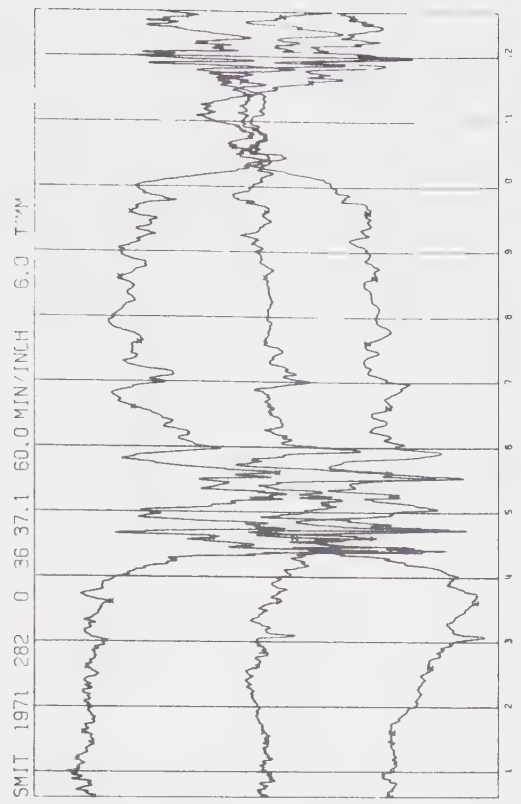
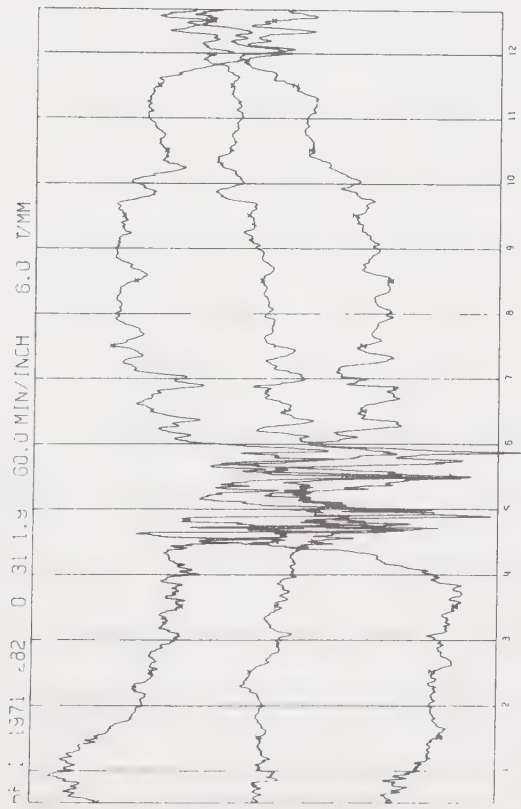


Figure 3.8

Event 25 (October 9, 1971, 0501-0510 UT) presents a different situation. Here we have a very clear double westward current system, which decays during the course of the event. The arcs are associated with the more northward one of the two current systems (see Figure 3.5). The boundary between the two current systems, as much as it is possible to identify one, appears to move southward with the arcs during the event.

Event 37 (October 29, 1971, 0420-0430 UT) is also associated with a double current system (Figure 3.6). However, it is more complicated than event 25, in that both systems involved here are of approximately equal strength, resulting in a very greatly distorted profile. We note that this double current system also decays by the end of the event. We can identify a general southward motion of the current system as the arcs drift south, but the distortion makes it impossible to determine anything more definite.

Not all events were as complex as the foregoing. As an example, we have event 19 (October 8, 1971, 0450-0456 UT) (Figure 3.7) for which the latitude profile behaves in the standard manner, except for the extremely large negative ΔD regime poleward of the electrojet. As mentioned, this is indicative of enhanced polar cap

convection. In this case, the very large negative ΔD is associated with an ionospheric electric field of 26 mV/m, which is a good deal higher than the average value of 16 mV/m.

4. DISCUSSION AND CONCLUSIONS

4.1 Mozer's Model

Mozer (1971) has proposed a model of magnetospheric substorms based on the behaviour of magnetospheric electric fields during substorms. Briefly, this model states that a westward electric field is created in the magnetotail due to the connection of interplanetary magnetic field lines with the Earth's dipole field lines at the magnetopause during periods when the interplanetary magnetic field has a southward pointing component. This electric field, which appears approximately an hour before the onset of the substorm, is then responsible for the inward convection of plasma in the magnetotail. The speed of this convection is given by E/B (as has been shown here). Since the electric field is constant to within a factor of 2 over the range $L = 4$ to $L = 9$ (Mozer and Manka, 1971), the speed of inward convection is inversely proportional to the strength of the magnetic field. This inverse dependence results in a build-up of plasma at locations of strongest magnetic field strength, namely, around the local midnight sector deep in the magnetosphere. After a sufficient time, the pressure gradients which result from this build-up of plasma initiate a plasma instability, and the plasma is

precipitated. The auroral arcs that are generated from this particle precipitation then drift equatorward. Thus, this model predicts the occurrence of equatorward drifting auroral arcs prior to the onset of a magnetic substorm, that is, during the growth phase of a substorm. It is clear that this prediction is a direct consequence of the fact that the westward electric field is present approximately an hour before the substorm, and the assumption that precipitation results from the instabilities caused by the plasma pressure gradients.

4.2 The Kennel-Petschek Mechanism

Brice (1970) has suggested that an injection of cold plasma into the magnetosphere could result in the sudden subjection of keV particles to the stable trapping limit proposed by Kennel and Petschek (1966).

The Kennel-Petschek theory is based on the fact that the precipitation of energetic electrons into the ionosphere is apparently a result of first adiabatic invariant violation. Such a violation requires time variations in the magnetic field of the order of the electron cyclotron frequency; it therefore appears that high-frequency fluctuations in the whistler mode are the most probable cause of the violation of the first adiabatic invariant. The injection of the cold plasma enhances

the whistler mode turbulence. It has been observed that the whistler mode is unstable for a sufficiently anisotropic pitch angle distribution (Cornwall, 1965). Hence, if an anisotropic pitch angle distribution is maintained, wave energy can be generated in the magnetosphere.

The stability of the wave growth depends primarily on particles in cyclotron resonance. In a spatially finite plasma, to maintain a self-sustaining pitch angle diffusion, both escaping particles and waves must be replaced. We see that the number of resonant particles must then adjust by balancing the acceleration and precipitation of particles to ensure that the wave growth rate exactly replaces the escaping wave energy. Clearly, a growth rate that is too large will create an accumulation of wave energy, which enhances particle precipitation; this, in turn, reduces the growth rate to the value necessary to maintain a steady-state distribution of the waves. Therefore, there is an upper limit to the stably trapped particle flux. However, the characteristic energy for cyclotron interactions is the magnetic energy per particle; hence this limit applies only to particles whose energy is greater than a threshold energy E_T , given by

$$E_T \propto \frac{B^2}{2\mu_0 N}$$

where B is the magnetic field strength, μ_0 is the

permeability of free space, and N is the ambient particle number density.

Hence, an injection of cold plasma into a volume of energetic plasma would decrease the threshold energy E_T to a lower value E_T' . This results in a larger number of particles, having energies greater than the new threshold energy E_T' ; thus a greater energy range of particles are brought under the conditions for the stable trapping limit.

4.3 Proposed Mechanism of Auroral Particle Precipitation

Vasyliunas (1968) and Frank (1968) have shown that the plasma sheet has a sharp and well-defined inner edge in the nightside magnetosphere, which moves inwards during periods of substorm activity. This boundary is comprised of a region of low energy electrons, whose number density is the same as that observed in the interior of the plasma sheet. Siscoe and Cummings (1969) have suggested that the inward motion of the inner edge of the plasma sheet occurs prior to the substorm. In their theory, there is a balance between the force exerted on the magnetotail by the solar wind, and the force between the Earth and the magnetotail. The tangential stress between the magnetotail and the solar wind is responsible for moving

magnetic flux into the tail. The magnetic flux is stored in the tail and returns to the magnetosphere at lower latitudes, but at a slower rate than the rate at which it is stored (Axford, 1965). As the tail flux increases, the normal pressure on the tail remains almost constant, and is balanced by the force on the tail from the solar wind. To accommodate the increase in flux, the radius of the tail increases, and the inner edge of the plasma sheet moves Earthward. This inward motion occurs during the build-up process in the tail, that is, prior to the onset of the substorm. The inward motion is stopped when the tangential stress on the tail is not balanced by the force on the Earth. At this stage the substorm is initiated and the plasma sheet reestablishes itself back in the magnetotail. The process repeats itself at the end of the substorm, if the driving force on the tail is still active.

The inward motion of the inner edge of the plasma sheet is accompanied by a thinning of the plasma sheet (Hones et al, 1967) and a build-up of the asymmetric ring current in the evening sector (Cummings et al, 1968). It has been proposed by Atkinson (1970) that the inward convecting plasma will be precipitated into the auroral zone ionosphere through the Kennel-Petschek mechanism of pitch angle scattering.

We now propose a model for the generation of equatorward drifting auroral arcs, based on the theoretical and observational material presented in this and the previous sections. During the pre-substorm period, the energetic electron population ($E > 1$ kev) would be so low as to be below the threshold level necessary for violation of the stable trapping limit even were the threshold energy E_T to be attained. Thus the inward motion of the plasma sheet would not be associated with precipitation of energetic electrons, and thus no equatorward drifting arcs would be observed. During the expansive phase of the substorm, an azimuthally confined sector of auroral arcs would expand poleward creating a distorted region known as the auroral bulge (Akasofu, 1964). Only an azimuthally confined portion of the plasma sheet which maps into the auroral bulge will be distorted such that its Earthward edge will be forced back into the tail. There is considerable evidence that substorms occur in confined azimuthal sectors as observed both in the magnetotail and at the Earth's surface (Rostoker and Camidge, 1971). Thus it should be clear that the inner edge of the plasma sheet will be further from the Earth in the substorm-distorted region than on either side of it.

During the period of the expansive phase after the arcs have reached their most poleward direction, the

bright auroral arcs are confined to the northern border of the auroral oval. This northern border is quite latitudinally confined and therefore maps into a rather limited range of L shells. It is on this limited range of the shells that the population of auroral electrons is energized. During the final stages of the expansive phase, the plasma sheet particles will gradient drift into the region of the magnetosphere which maps into the auroral bulge region in the ionosphere.

When the decay phase starts, the energetic electrons at the northern border of the oval are $\underline{E} \times \underline{B}$ drifted Earthward (under the action of the tail electric field) into the warm plasma sheet particles which have gradient drifted in equatorward of the L -shell populated by the energetic electrons. This warm plasma has densities of $0.4\text{--}25 \text{ cm}^{-3}$ (Vasyliunas, 1968), and this may easily cause the characteristic energy E_T to drop to encompass the auroral electron energy range of $1\text{--}10 \text{ keV}$. The enveloping of the hot plasma (from the L -shell) in the relatively cooler plasma in the ring current has the same effect as that proposed by Brice (1970). The Kennel-Petschek stable trapping limit is then violated and precipitation results, causing the generation of the auroral arcs. The L -shell of energetic electrons is simultaneously convected inwards and precipitating electrons. This results in the apparent equatorward

motion of the auroral arcs generated by the precipitation. This view of the generating mechanism of the equatorward drifting arcs is supported to some extent by the fact that the average speed of inward motion of the inner edge of the plasma sheet between $10 R_E$ and $6 R_E$ is ~ 12 km/sec (Vasyliunas, 1968), which maps into the ionosphere as an average velocity of ~ 530 m/sec. This value compares favorably with the most probable range of drift velocities in this study which lies between 400-600 m/sec.

From this theory, one would not expect southward drifting arcs during the growth phase of a substorm. When the plasma sheet moves inward prior to the substorm, the energetic particle population in the nightside magnetosphere is not large enough for the stable trapping limit to be violated. The occurrence of the substorm results in the energization of large numbers of particles, so that the subsequent inward motion of these energetic particles through a region near the Earthward edge of the plasma sheet would result in continual precipitation of auroral particles until the auroral electron population dropped below the stable trapping limit. Thus southward drifting arcs would be associated with the recovery phase of a magnetic substorm. This is confirmed by our observational findings.

In spite of the foregoing arguments, there is still a possible case that southward drifting arcs could be

associated with the growth phase of a substorm. The theory presented here is based on the following model of a magnetic substorm: During the development phase of the substorm the plasma sheet moves Earthward under the action of the convective force in the magnetotail. Due to the low flux of trapped energetic particles in the nightside magnetosphere, particle precipitation is not very likely at this stage. During the substorm activity, some of these trapped particles are accelerated so that their energy exceeds the threshold energy E_T and their large flux at this time makes them subject to the stable trapping limit. After the expansive phase of the substorm, the inner edge of the plasma sheet in an azimuthally confined region will reestablish itself further back in the magnetotail. At this stage, that is, the recovery phase of the substorm, the distortion of the inner edge of the plasma sheet disappears and the energized electrons at the edge of the auroral bulge would thus be governed by the stable trapping limit.

However, in the magnetosphere, the inward motion of the plasma sheet associated with the growth phase is identical in character to the inward motion of the re-established plasma sheet and regions of enhanced energetic electron population associated with the recovery phase. The second inward motion may thus conceivably be identified

as the growth phase for subsequent substorm activity; in this case the growth phase would have associated southward drifting arcs. Therefore, the apparent contradiction between our results and those of Mozer (1971) and Feldstein (1972) is due in fact to the existing ambiguity in differentiating between a growth and recovery phase of a magnetic substorm. Despite this ambiguity, it is clear that no southward drifting arcs would appear during the growth phase of an isolated substorm, or prior to the onset of a period of sustained substorm activity.

It is important to point out that the second inward motion of the plasma sheet may or may not occur, depending on the continued existence of the enhanced convection electric field. Thus we will not always have southward drifting arcs associated with the recovery phase of the substorm. Another possibility is that there is a lapse of time between the first and second inward motions of the plasma sheet. We would then still have particle precipitation during the second inward motion of the plasma sheet, since our mechanism is not time dependent, but depends only on the trapped particle flux. (It should be noted that if the "lapse of time" is of any considerable extent, the energetic trapped particle population is likely to move out of the potential precipitating zone, due to the gradient drift of the electrons).

4.4 Conclusions

Assuming the validity of the theory of particle precipitation presented here, it is at once clear that the velocity of southward drift of the arcs is directly related to the value of the ionospheric electric field; the electric field value may then be inferred from the drift velocity of the arcs (Kelley et al, 1971). The validity of this relationship is shown by the agreement of the electric field values obtained in this manner, with the values obtained by other methods, such as balloon measurements (Mozer and Manka, 1971), barium cloud techniques (Haerendel and Lüst, 1970), and whistler techniques (Carpenter et al, 1972).

The evidence of the magnetic records associated with the auroral events showed that during a sample time of fifteen months and over a total of 43 events of southward drifting arcs, there was not one instance where southward drifting arcs were associated with the growth phase of the associated polar magnetic substorm. This is consistent with the view that there are not large fluxes of trapped energetic particles in the outer region of the nightside quiet-time magnetosphere. Hence, the immersion of regions populated by auroral electrons in the plasma sheet will not produce precipitation of those energetic electrons if their population is below the stable trapping

limit. Only after substorm activity has resulted in the acceleration of large numbers of energetic electrons, would their population be large enough to be stimulated by the Kennel-Petschek mechanism causing particle precipitation and the generation of auroral arcs. The fact that 34 of the 43 events were associated with the recovery phase of a substorm, and none with the development phase, shows that the appearance of southward drifting arcs is an invalid auroral signature for the growth phase of a magnetic substorm, unless one considers that the growth phase and recovery phase may coexist after a period of earlier substorm activity.

BIBLIOGRAPHY

- Akasofu, S. -I., The development of the auroral substorm, *Planet. Space Sci.* 12, 273, 1964.
- Akasofu, S. -I., D. Kimball and C. -I. Meng, Dynamics of the aurora - VII equatorward motions and the multiplicity of auroral arcs, *J. Atmos. Terrest. Phys.* 28, 623, 1966b.
- Akasofu, S. -I., Polar and Magnetospheric Substorms, Springer-Verlag, New York, 1968.
- Atkinson, G., Auroral arcs: result of the interaction of a dynamic interaction of a dynamic magnetosphere with the ionosphere, *J. Geophys. Res.* 75, 4746, 1970.
- Axford, W. I., Magnetic storm effects associated with the tail of the magnetosphere, paper presented at *ESRO Conf. on the Magnetosphere*, November, 1965.
- Belyakova, S. I., S. A. Zaytseva and M. I. Pudovkin, Development of a polar storm, *Geomag. and Aeron.* 8, 569, 1968.
- Brice, N. M., Artificial enhancement of energetic particle precipitation through cold plasma injection: a technique for seeding substorms? *J. Geophys. Res.* 75, 4890, 1970.
- Brice, N. and C. Lucas, Influence of magnetospheric convection and polar wind on loss of electrons from the outer radiation belt, *J. Geophys. Res.* 76, 900, 1971.
- Carpenter, D. L., K. Stone, J. C. Siren and T. L. Crystal, Magnetospheric electric fields deduced from drifting whistler paths, *J. Geophys. Res.* 77, 2819, 1972.
- Chen, A. J. and R. A. Wolf, On the theoretical interpretation of the plasmasphere's bulge, *EOS Trans. Am. Geophys. Union* 54, 462, 1972.

- Cornway, J. M., Cyclotron instabilities and electromagnetic emission in the ultralow frequency and very low frequency ranges, *J. Geophys. Res.* 70, 61, 1965.
- Cornwall, J. M., F. V. Coroniti and R. M. Thorne, A unified theory of SAR arc formation at the plasmapause, *J. Geophys. Res.* 76, 4428, 1971.
- Cummings, W. D., J. N. Barfield and P. J. Coleman, Magnetospheric substorms observed at the synchronous orbit, *J. Geophys. Res.* 73, 6687, 1968.
- Davis, T. N., Evidence of convective motion in the outer magnetosphere, *EOS Trans. AGU* 42, 219, 1962.
- Davis, T. N., Magnetospheric convection pattern inferred from magnetic disturbance and auroral motions, *J. Geophys. Res.* 76, 5978, 1971.
- Feldstein, Y. I., Auroras and associated phenomena, *Solar-Terrestrial Physics/1970 Part III*, p. 152, ed. E. R. Dyer, D. Reidel Publ. Co., Dordrecht, Holland, 1972.
- Frank, L. A., On the distribution of low energy protons and electrons in the earth's magnetosphere, in: Earth's Particles and Fields, ed. B. M. McCormac, p. 67, Reinhold, New York, 1968.
- Haerendel, G. and R. Lüst, Electric fields in the ionosphere and magnetosphere, in: Particles and Fields in the Magnetosphere, ed. B. M. McCormac, p. 213, D. Reidel Publ. Co., Dordrecht, Holland, 1970.
- Hones, E. W., J. R. Asbridge, S. J. Bame and I. B. Strong, Outward flow of plasma in the magnetotail following geomagnetic bays, *J. Geophys. Res.* 72, 5879, 1967.
- Kelley, M. C., J. A. Starr and F. S. Mozer, Relationship between magnetospheric electric fields and the motion of auroral forms, *J. Geophys. Res.* 76, 5269, 1971.
- Kennel, C. F. and H. E. Petschek, Limit on stably trapped particle fluxes, *J. Geophys. Res.* 71, 1, 1966.

- Kisabeth, J. L., The dynamical development of the polar electrojets, *Ph.D. Thesis*, Univ. of Alberta, Fall, 1972.
- Kisabeth, J. L. and G. Rostoker, Development of the polar electrojet during polar magnetic substorms, *J. Geophys. Res.* 76, 6815, 1971.
- McPherron, R. L., Growth phase of magnetospheric substorms, *J. Geophys. Res.* 75, 5592, 1970.
- Mozer, F. S., Electric field mapping in the ionosphere at the equatorial plane, *Planet. Space Sci.* 18, 259, 1970.
- Mozer, F. S., Origin and effects of electric fields during isolated magnetospheric substorms, *J. Geophys. Res.* 76, 7595, 1971.
- Mozer, F. S. and R. H. Manka, Magnetospheric electric field properties deduced from simultaneous balloon flights, *J. Geophys. Res.* 76, 1697, 1971.
- Roederer, J. G., Dynamics of Geomagnetically Trapped Radiation, *Springer-Verlag*, New York, 1970.
- Rostoker, G. and F. P. Camidge, The localized character of magnetotail magnetic fluctuations during polar magnetic substorms, *J. Geophys. Res.* 76, 6944, 1971.
- Siscoe, G. L. and W. D. Cummings, On the cause of geomagnetic bays, *Planet. Space Sci.* 17, 1795, 1969.
- Vasyliunas, V. M., A survey of low energy electrons in the evening sector of the magnetosphere withOGO 1 and OGO 3, *J. Geophys. Res.* 73, 2839, 1968.
- Vasyliunas, V. M., Penetration of convection into the inner magnetosphere, *EOS Trans. Am. Geophys. Union* 53, 461, 1971.

TABLE A1 : LIST OF EVENTS

Times for all events are given in UT (LT+7). The linear mapping is accurate to 250 km to the north and south of the zenith. For convenience of notation, the northern direction has been arbitrarily designated positive along the longitudinal axis, and the southern direction negative. The origin of the co-ordinate system is the zenith. Thus an arc whose location is -100 km with a velocity of -400 m/sec is 100 km south of the zenith and travelling southward with a speed of 400 m/sec.

List of Events

Event 1 : July 28, 1970 (Day 209)

Time(UT)	Location (km)	Velocity (m/sec)
0834	146	
0835	138	-133
0836	134	- 66.7
0837	119	-250

$$\bar{v}_1 = -149.9 \text{ m/sec.}$$

Event 2 : July 28, 1970 (Day 209)

Time (UT)	Location (km)	Velocity (m/sec)
0839	138	
0840	125	-217
0841	113	-200

$$\bar{v}_2 = -208.5 \text{ m/sec.}$$

Event 3 : September 22, 1970 (Day 265)

Time (UT)	Location (km)	Velocity (m/sec)
1047	-69	
1048	-67	33.3
1049	-75	-300
1050	-91	-267
1051	-94	- 50
1052	-105	-183
1053	-110	- 83
1054	-120	-167
1055	-135	-250
1056	-140	- 83

$$\bar{v}_3 = -165.4 \text{ m/sec.}$$

Event 4 : October 12, 1970 (Day 285)

Time (UT)	Location (km)	Velocity (m/sec)
0427	- 28	
0428	- 44	-267
0429	- 94	-833
0430	-105	-183

$$\bar{v}_4 = -506.6 \text{ m/sec.}$$

Event 5 : October 12, 1970 (Day 285)

Time (UT)	Location (km)	Velocity (m/sec)
0711	- 88	
0712	- 81	117
0713	- 94	-217
0714	-110	-267
0715	- 47	1050

$$\bar{v}_5 = -242 \text{ m/sec.}$$

Event 6 : October 15, 1970 (Day 288)

Time (UT)	Location (km)	Velocity (m/sec)
0802	- 97	
0803	-110	-217
0804	-115	- 83
0805	-115	0

$$\bar{v}_6 = -150 \text{ m/sec.}$$

Event 7 : October 15, 1970 (Day 288)

Time (UT)	Location (km)	Velocity (m/sec)
0943	-19	
0944	-50	-517
0945	-81	-517
0946	-68	217
0947	-97	-483

$$\bar{v}_7 = -505.7 \text{ m/sec.}$$

Event 8 : October 24, 1970 (Day 297)

Time (UT)	Location (km)	Velocity (m/sec)
0605	69	
0606	53	-267
0607	25	-467
0608	-10	-587
0609	-20	-167
0610	-50	-500

$$\bar{v}_8 = -397.6 \text{ m/sec.}$$

Event 9 : October 25, 1970 (Day 298)

Time (UT)	Location (km)	Velocity (m/sec)
0729	-110	
0730	-190	-1333
0731	-215	- 417
0732	-220	- 83
0733	-120	1667

$$\bar{v}_9 = -611.0 \text{ m/sec.}$$

Event 10 : October 25, 1970 (Day 298)

Time (UT)	Location (km)	Velocity (m/sec)
0740	141	
0741	100	-683
0742	69	-517
0743	50	-317

$$\bar{v}_{10} = -505.7 \text{ m/sec.}$$

Event 11 : November 3, 1970 (Day 307)

Time (UT)	Location (km)	Velocity (m/sec)
0745	184	
0746	175	-150
0747	159	-267

$$\bar{v}_{11} = -208.5 \text{ m/sec.}$$

Event 12 : November 5, 1970 (Day 309)

Time (UT)	Location (km)	Velocity (m/sec)
0838	172	
0839	281	1817
0840	141	-2333
0841	103	- 633
0842	91	- 200

$$\bar{v}_{12} = -1022.0 \text{ m/sec.}$$

Event 13 : February 23, 1971 (Day 54)

Time (UT)	Location (km)	Velocity (m/sec)
0650	- 40	
0651	- 60	- 333.3
0652	- 79	- 316.7
0653	-102	- 383.3
0654	-102	0.0
0655	-130	- 466.7
0656	-221	-1516.7

$$\bar{v}_{13} = -502.8 \text{ m/sec.}$$

Event 14 : October 8, 1971 (Day 281)

Time (UT)	Location (km)	Velocity (m/sec)
0331	257	
0332	220	- 616.7
0333	193	- 450.0
0334	115	-1300.0
0335	114	- 16.7
0336	91	- 383.3
0337	60	- 516.7
0338	27	- 550.0
0339	20	- 116.7
0340	-20	- 666.7

$$\bar{v}_{14} = -513.0 \text{ m/sec.}$$

Event 15 : October 8, 1971 (Day 281)

Time (UT)	Location (km)	Velocity (m/sec)
0346	220	
0347	149	-1183.3
0348	145	- 66.7
0349	121	- 400.0
0350	120	- 16.7
0351	100	- 333.3
0352	60	- 666.7
0353	27	- 550.0
0354	10	- 283.3

$$\bar{v}_{15} = -437.5 \text{ m/sec.}$$

Event 16 : October 8, 1971 (Day 281)

Time (UT)	Location (km)	Velocity (m/sec)
0350	218	
0351	188	- 500.0
0352	160	- 466.7
0353	147	- 216.7
0354	181	566.7

$$\bar{v}_{16} = -394.5 \text{ m/sec.}$$

Event 17 : October 8, 1971 (Day 281)

Time (UT)	Location (km)	Velocity (m/sec)
0445	242	
0446	236	-100.0
0447	195	-683.3
0448	175	-333.3
0449	142	-550.0
0450	110	-533.3
0451	101	-150.0
0452	80	-350.0
0453	70	-166.7
0454	70	0.0
0455	49	-350.0

$$\bar{v}_{17} = -321.7 \text{ m/sec.}$$

Event 18 : October 8, 1971 (Day 281)

Time (UT)	Location (km)	Velocity (m/sec)
0450	50	
0451	49	- 16.7
0452	0	-816.7
0453	0	0.0
0454	0	0.0
0455	- 1	- 16.7
0456	0	16.7
0457	-20	-333.3
0458	-38	-300.0

Event 18 : October 8, 1971 (Day 281) - continued

Time (UT)	Location (km)	Velocity (m/sec)
0459	- 51	- 216.7
0500	-130	-1316.7

$$\bar{v}_{18} = -335.2 \text{ m/sec.}$$

Event 19 : October 8, 1971 (Day 281)

Time (UT)	Location (km)	Velocity (m/sec)
0450	32	
0451	5	- 450.0
0452	- 57	-1033.3
0453	- 90	- 550.0
0454	-132	- 700.0
0455	-159	- 450.0
0456	-231	-1200.0

$$\bar{v}_{19} = -730.6 \text{ m/sec.}$$

Event 20 : October 9, 1971 (Day 282)

Time (UT)	Location (km)	Velocity (m/sec)
0250	110	
0251	94	- 266.7
0252	81	- 116.7
0253	59	- 366.7
0254	28	- 516.7
0255	100	1200.0
0256	-10	-1833.3

$$\bar{v}_{20} = -620.0 \text{ m/sec.}$$

Event 21 : October 9, 1971 (Day 282)

Time (UT)	Location (km)	Velocity (m/sec)
0250	-28	
0251	-38	-166.7
0252	-50	-200.0
0253	-60	-166.7
0254	-78	-300.0
0255	-71	166.7
0256	-83	-200.0

$$\bar{v}_{21} = -206.7 \text{ m/sec.}$$

Event 22 : October 9, 1971 (Day 282)

Time (UT)	Location (km)	Velocity (m/sec)
0307	58	
0308	10	-800.0
0309	- 7	-283.3
0310	-38	-516.7
0311	-58	-333.3
0312	-89	-516.7
0313	-80	150.0
0314	-99	-316.7

$$\bar{v}_{22} = -461.1 \text{ m/sec.}$$

Event 23 : October 9, 1971 (Day 282)

Time (UT)	Location (km)	Velocity (m/sec)
0313	59	
0314	51	-133.3
0315	30	-350.0
0316	- 2	-533.3
0317	- 2	0.0
0318	- 2	0.0
0319	-28	-433.3
0320	-19	150.0
0321	-20	- 16.7
0322	-31	-183.3
0323	-41	-166.7
0324	-41	0.0
0325	-40	16.7
0326	-60	-333.3
0327	---	---
0328	-99	-325.0
0329	-112	-216.7
0330	-140	-466.7

$$\bar{v}_{23} = -225.6 \text{ m/sec.}$$

Event 24 : October 9, 1972 (Day 282)

Time (UT)	Location (km)	Velocity (m/sec)
0323	77	
0324	62	-250.0
0325	54	-133.3
0326	44	-166.7
0327	- 4	-800.0
0328	0	66.7
0329	-38	-633.3
0330	-60	-360.7

$$\bar{v}_{24} = -391.7 \text{ m/sec.}$$

Event 25 : October 9, 1971 (Day 282)

Time (UT)	Location (km)	Velocity (m/sec)
0501	221	
0502	189	- 533.3
0503	38	-2516.7
0504	-40	-1300.0
0505	-79	- 650.0
0506	-90	- 183.3
0507	-145	- 916.7
0508	-163	- 300.0
0509	-200	- 616.7
0510	-280	-1333.3

$$\bar{v}_{25} = -927.8 \text{ m/sec.}$$

Event 26 : October 9, 1971 (Day 282)

Time (UT)	Location (km)	Velocity (m/sec)
0652	228	
0653	140	-1466.7
0654	123	- 283.3
0655	99	- 400.0
0656	52	- 783.3
0657	- 2	- 900.0
0658	-60	- 966.7
0659	-120	-1000.0
0700	-210	-1500.0
0701	-150	1000.0
0702	-198	- 800.0

$$\bar{v}_{26} = -900 \text{ m/sec.}$$

Event 27 : October 9, 1972 (Day 282)

Time (UT)	Location (km)	Velocity (m/sec)
0700	194	
0701	170	- 400.0
0702	139	- 516.7
0703	90	- 816.7
0704	44	- 766.7
0705	20	- 400.0
0706	8	- 200.0

$$\bar{v}_{27} = -516.7 \text{ m/sec.}$$

Event 28 : October 9, 1971 (Day 282)

Time (UT)	Location (km)	Velocity (m/sec)
0837	132	
0838	91	-683.3
0839	51	-666.7
0840	38	-216.7
0841	-19	-950.0
0842	-25	-100.0
0843	-29	- 66.7
0844	-41	-200.0
0845	-82	-683.3
0846	-97	-250.0
0847	-108	-183.3
0848	-130	-366.7
0849	-140	-166.7
0850	-159	-316.7

$$\bar{v}_{28} = -373.1 \text{ m/sec.}$$

Event 29 : October 9, 1971 (Day 282)

Time (UT)	Location (km)	Velocity (m/sec)
0901	-79	
0902	-93	-233.3
0903	-118	-416.7
0904	-140	-366.7
0905	-196	-933.3

$$\bar{v}_{29} = -487.5 \text{ m/sec.}$$

Event 30 : October 9, 1971 (Day 282)

Time (UT)	Location (km)	Velocity (m/sec)
0923	-39	
0924	-61	- 366.7
0925	-77	- 266.7
0926	-80	- 50.0
0927	-118	- 633.3
0928	-118	0.0
0929	-200	-1366.7
0930	-282	-1366.7

$$\bar{v}_{30} = -578.6 \text{ m/sec.}$$

Event 31 : October 9, 1971 (Day 282)

Time (UT)	Location (km)	Velocity (m/sec)
1105	14	
1106	-54	-1133.3
1107	-63	- 150.0
1108	-79	- 266.7
1109	-90	- 183.3

$$\bar{v}_{31} = -433.3 \text{ m/sec.}$$

Event 32 : October 22, 1971 (Day 295)

Time (UT)	Location (km)	Velocity (m/sec)
0724	133	
0725	117	-266.7
0726	117	0.0
0727	90	-450.0
0728	48	-700.0
0729	-11	-983.3

$$\bar{v}_{32} = -480.0 \text{ m/sec.}$$

Event 33 : October 24, 1971 (Day 297)

Time (UT)	Location (km)	Velocity (m/sec)
0535	180	
0536	122	-966.7
0537	91	-350.0
0538	59	-533.3
0539	40	-316.7
0540	12	-466.7
0541	-20	-533.3
0542	-60	-666.7
0543	-110	-833.3
0544	-208	-1633.3
0545	-259	-850.0

$$\bar{v}_{33} = -715.0 \text{ m/sec.}$$

Event 34 : October 24, 1971 (Day 297)

Time (UT)	Location (km)	Velocity (m/sec)
0538	120	
0539	92	-466.7
0540	102	166.7
0541	60	-700.0
0542	44	266.7
0543	- 2	-766.7
0544	-48	-766.7
0545	-80	-533.3

$$\bar{v}_{34} = -455.6 \text{ m/sec.}$$

Event 35 : October 24, 1971 (Day 297)

Time (UT)	Location (km)	Velocity (m/sec)
0842	95	
0843	70	-416.7
0844	68	- 33.3
0845	42	-433.3
0846	30	-133.3
0847	3	-450.0
0484	0	- 50.0
0849	-20	-333.3
0850	-42	-366.7
0851	-57	-250.0

$$\bar{v}_{35} = -274.1 \text{ m/sec.}$$

Event 36 : October 28, 1971 (Day 301)

Time (UT)	Location (km)	Velocity (m/sec)
0920	98	
0921	73	-416.7
0922	35	-633.3
0923	- 9	-733.3
0924	-49	-666.7
0925	-80	-516.7
0926	-83	- 50.0

$$\bar{v}_{36} = -502.8 \text{ m/sec.}$$

Event 37 : October 29, 1971 (Day 302)

Time (UT)	Location (km)	Velocity (m/sec)
0420	77	
0421	56	-350.0
0422	41	-250.0
0423	9	-533.3
0424	-20	-483.3
0425	-30	-166.7
0426	-30	0.0
0427	-38	-133.3
0428	-60	-366.7
0429	-69	-150.0
0430	-220	-2516.7

$$\bar{v}_{37} = -495.0 \text{ m/sec.}$$

Event 38 : October 29, 1971 (Day 302)

Time (UT)	Location (km)	Velocity (m/sec)
0429	-10	
0430	-42	-533.3
0431	-90	-800.0
0432	-93	- 50.0

$$\bar{v}_{38} = -461.1 \text{ m/sec.}$$

Event 39 : October 29, 1971 (Day 302)

Time (UT)	Location (km)	Velocity (m/sec)
0434	137	
0435	111	-433.3
0436	119	133.3
0437	100	-316.7
0438	90	-166.7

$$\bar{v}_{39} = -305.6 \text{ m/sec.}$$

Event 40 : October 29, 1971 (Day 302)

Time (UT)	Location (km)	Velocity (m/sec)
0438	199	
0439	162	-616.7
0440	160	- 33.3
0441	158	- 33.3
0442	139	-316.7
0443	122	-283.3

$$\bar{v}_{40} = -256.7 \text{ m/sec.}$$

Event 41 : October 29, 1971 (Day 302)

Time (UT)	Location (km)	Velocity (m/sec)
0444	179	
0445	155	-400.0
0446	155	0.0
0447	117	-633.3
0448	121	66.7
0449	122	16.7
0450	112	-166.7
0451	110	-200.0
0452	100	-166.7
0453	89	-183.3
0454	59	-500.0
0455	38	-350.0
0456	21	-283.3
0457	7	-233.3
0458	-51	-966.7

$$\bar{v}_{41} = -340.3 \text{ m/sec.}$$

Event 42 : October 29, 1971 (Day 302)

Time (UT)	Location (km)	Velocity (m/sec)
0456	69	
0457	47	-366.7
0458	22	-416.7
0459	19	- 50.0
0500	14	- 83.3

Event 42 : October 29, 1971 (Day 302) - continued

Time (UT)	Location (km)	Velocity (m/sec)
0501	20	100.0
0502	-18	-633.3
0503	8	433.3
0504	4	- 66.7
0505	- 3	-116.7

$$\bar{v}_{42} = -247.6 \text{ m/sec.}$$

Event 43 : October 30, 1971 (Day 303)

Time (UT)	Location (km)	Velocity (m/sec)
0310	248	
0311	240	-133.3
0312	235	- 83.3
0313	239	66.7
0314	201	-633.3
0315	203	33.3
0316	183	-333.3
0317	160	-383.3
0318	131	-483.3
0319	103	-1120.0
0320	100	- 50.0
0321	71	-483.3
0322	42	-483.3
0323	10	-533.3
0324	-12	-366.7

Event 43 : October 30, 1971 (Day 303) - continued

Time (UT)	Location (km)	Velocity (m/sec)
0325	-40	-466.7
0326	-60	-333.3
0327	-60	0.0

$$\bar{v}_{43} = -392.4 \text{ m/sec.}$$

TABLE A2 : SUMMARY OF RESULTS

Event No.	Date of Event	Time of Event (UT:=LT+7)	Ionospheric Velocity (m/sec)	Equatorial Plane Velocity (m/sec)	Equatorial Plane Elec- tric Field (mV/m)	Ionospheric Electric Field (mV/m)
1	July 28, 1970	0834-0837	-149.9	-2773	0.29	5
2	July 28, 1970	0839-0841	-208.5	-3857	0.41	8
3	Sept. 22, 1970	1047-1056	-165.4	-3060	0.32	6
4	Oct. 12, 1970	0427-0430	-506.6	-9372	0.99	18
5	Oct. 12, 1970	0711-0715	-242.0	-4477	0.47	9
6	Oct. 15, 1970	0802-0805	-150.0	-2775	0.29	5
7	Oct. 15, 1970	0943-0947	-505.7	-9356	0.00	18
8	Oct. 24, 1970	0605-0610	-397.6	-7356	0.78	14
9	Oct. 25, 1970	0729-0733	-611.0	-11304	1.19	22
10	Oct. 25, 1970	0740-0743	-505.7	-9356	0.99	18
11	Nov. 3, 1970	0745-0747	-208.5	-3857	0.41	8
12	Nov. 5, 1970	0838-0842	-1022.0	-18907	1.99	37
13	Feb. 23, 1971	0650-0656	-502.8	-9302	0.98	18
14	Oct. 8, 1971	0331-0340	-513.0	-9491	1.00	19
15	Oct. 8, 1971	0346-0354	-437.5	-8094	0.85	16

TABLE A2 : SUMMARY OF RESULTS (cont'd)

Event No.	Date of Event	Time of Event (UT:=LT+7)	Ionospheric Velocity (m/sec)	Equatorial Plane Velocity (m/sec)	Equatorial Plane Elec- tric Field (mV/m)	Ionospheric Electric Field (mV/m)
16	Oct. 8, 1971	0350-0354	-394.5	-7298	0.77	14
17	Oct. 8, 1971	0445-0455	-321.7	-5952	0.63	12
18	Oct. 8, 1971	0450-0500	-335.2	-6201	0.65	12
19	Oct. 8, 1971	0450-0456	-730.6	-13516	1.43	26
20	Oct. 9, 1971	0250-0256	-620.0	-11470	1.21	22
21	Oct. 9, 1971	0250-0256	-206.7	-3824	0.40	7
22	Oct. 9, 1971	0307-0314	-461.1	-8530	0.90	17
23	Oct. 9, 1971	0313-0330	-225.6	-4174	0.44	8
24	Oct. 9, 1971	0323-0330	-391.7	-7247	0.76	14
25	Oct. 9, 1971	0501-0510	-927.8	-17164	1.81	33
26	Oct. 9, 1971	0652-0702	-900.0	-16650	1.77	33
27	Oct. 9, 1971	0700-0706	-516.7	-9559	1.01	19
28	Oct. 9, 1971	0837-0850	-373.1	-6902	0.73	14
29	Oct. 9, 1971	0901-0905	-487.5	-9019	0.95	18
30	Oct. 9, 1971	0923-0930	-578.6	-10704	1.13	21

TABLE A2 : SUMMARY OF RESULTS (cont'd)

Event No	Date of Event	Time of Event (UT:=LT+7)	Ionospheric Velocity (m/sec)	Equatorial Plane Velocity (m/sec)	Equatorial Plane Elec- tric Field (mV/m)	Ionospheric Electric Field (mV/m)
31	Oct. 9, 1971	1105-1109	-433.3	-8016	0.85	16
32	Oct. 9, 1971	0724-0729	-480.0	-8880	0.94	17
33	Oct. 24, 1971	0535-0545	-715.0	-13228	1.40	26
34	Oct. 24, 1971	0538-0545	-455.6	-8429	0.89	16
35	Oct. 24, 1971	0842-0851	-274.1	-5071	0.53	10
36	Oct. 28, 1971	0920-0926	-502.8	-9302	0.98	18
37	Oct. 29, 1971	0420-0430	-495.0	-9158	0.97	18
38	Oct. 29, 1971	0429-0432	-461.1	-8530	0.90	17
39	Oct. 29, 1971	0434-0438	-305.6	-5654	0.60	11
40	Oct. 29, 1971	0438-0443	-256.7	-4749	0.50	9
41	Oct. 29, 1971	0444-0458	-340.3	-6296	0.66	12
42	Oct. 29, 1971	0456-0505	-247.6	-4581	0.48	9
43	Oct. 30, 1971	0310-0327	-392.4	-7259	0.77	14
Average Values			-440.8	-8156	0.86	16 ± 7

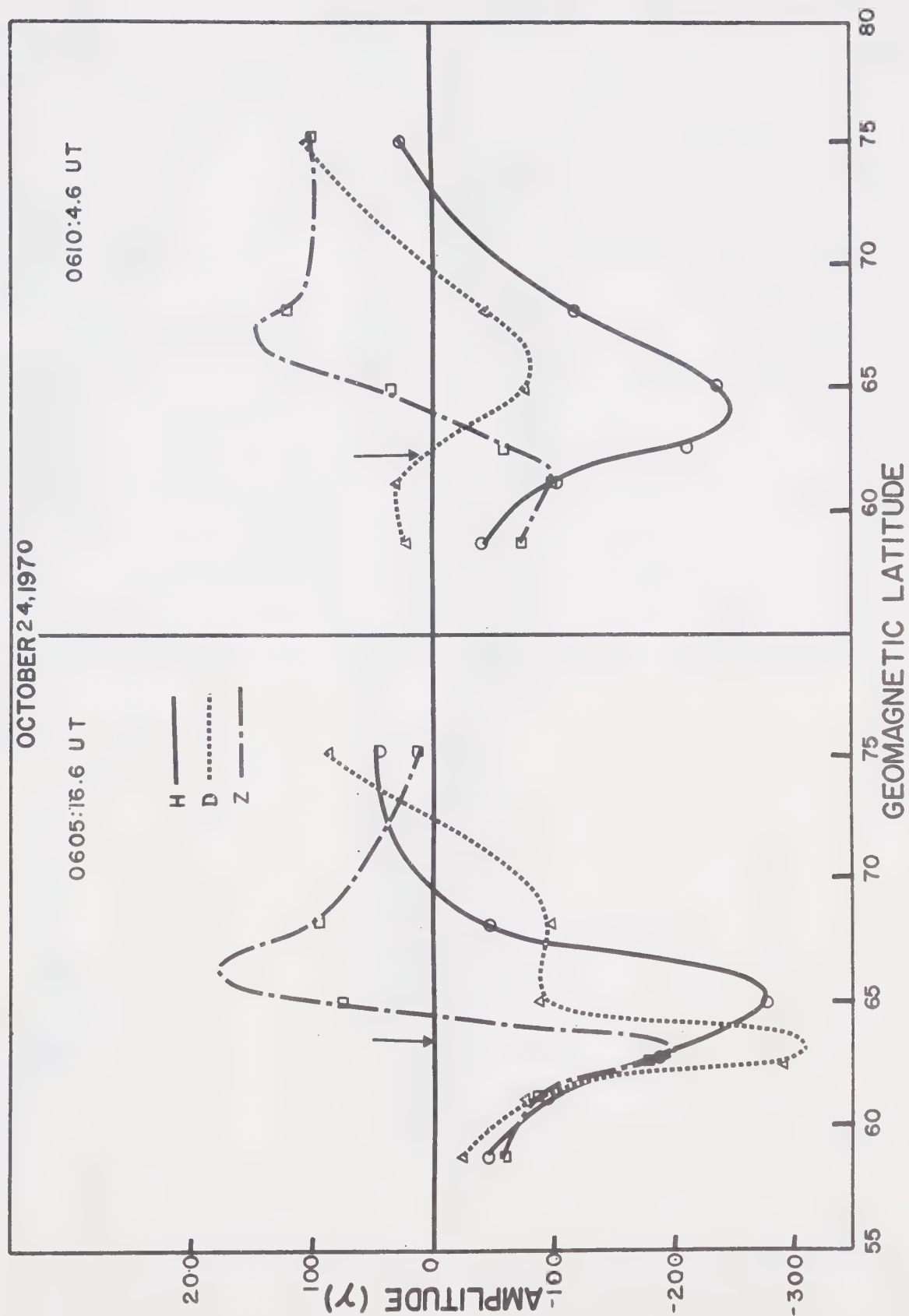


Figure Ala

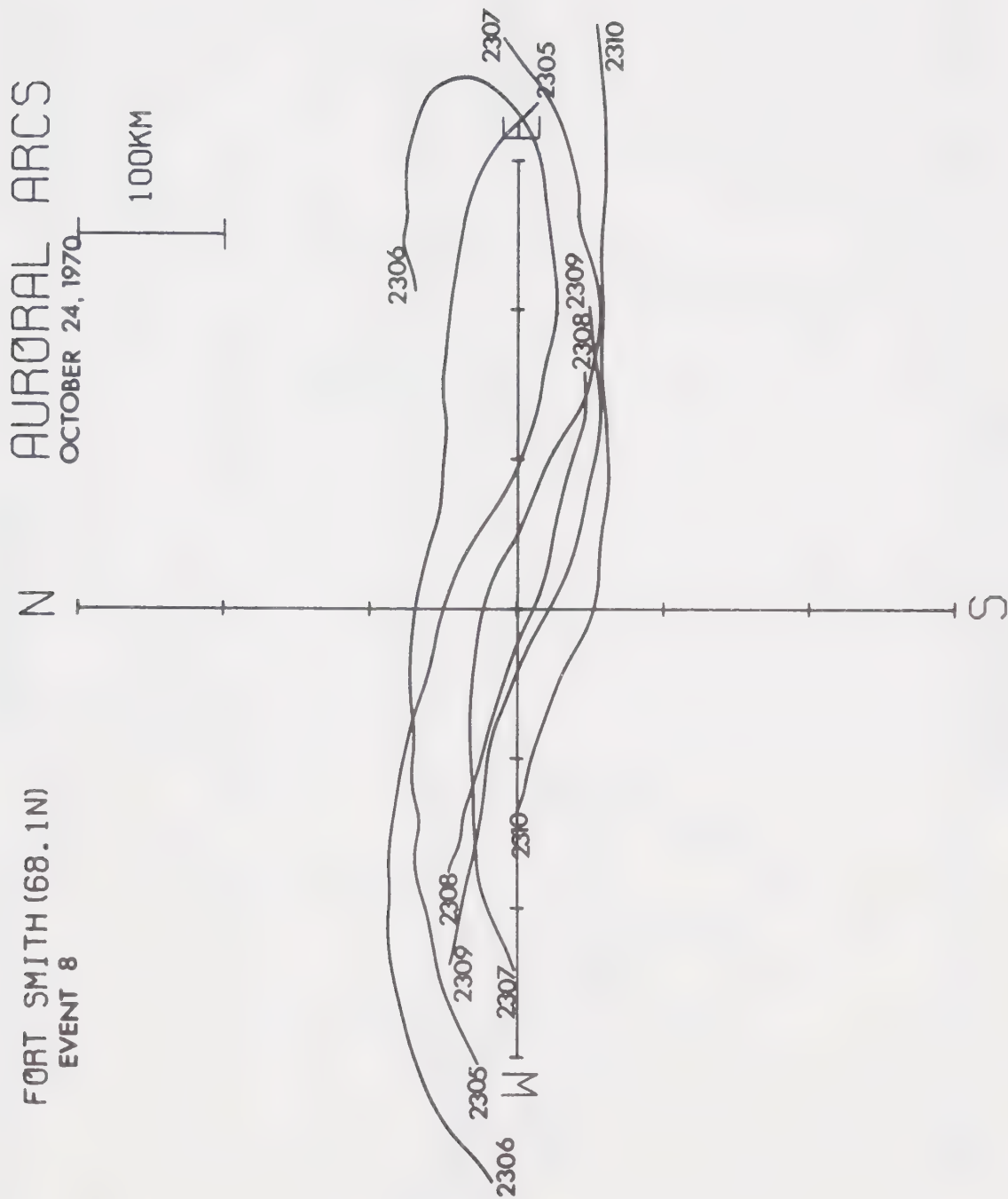


Figure Alb

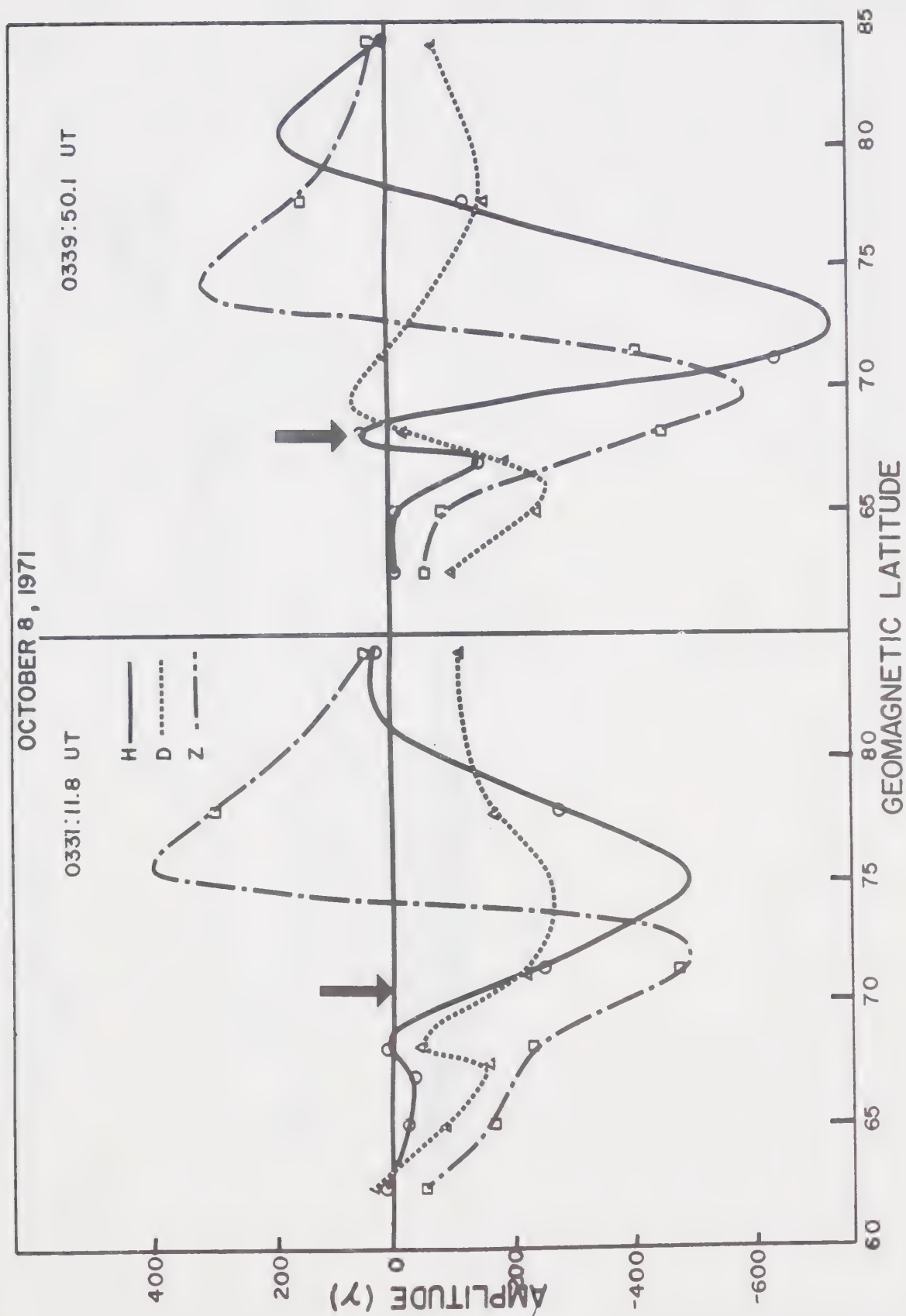


Figure A2a

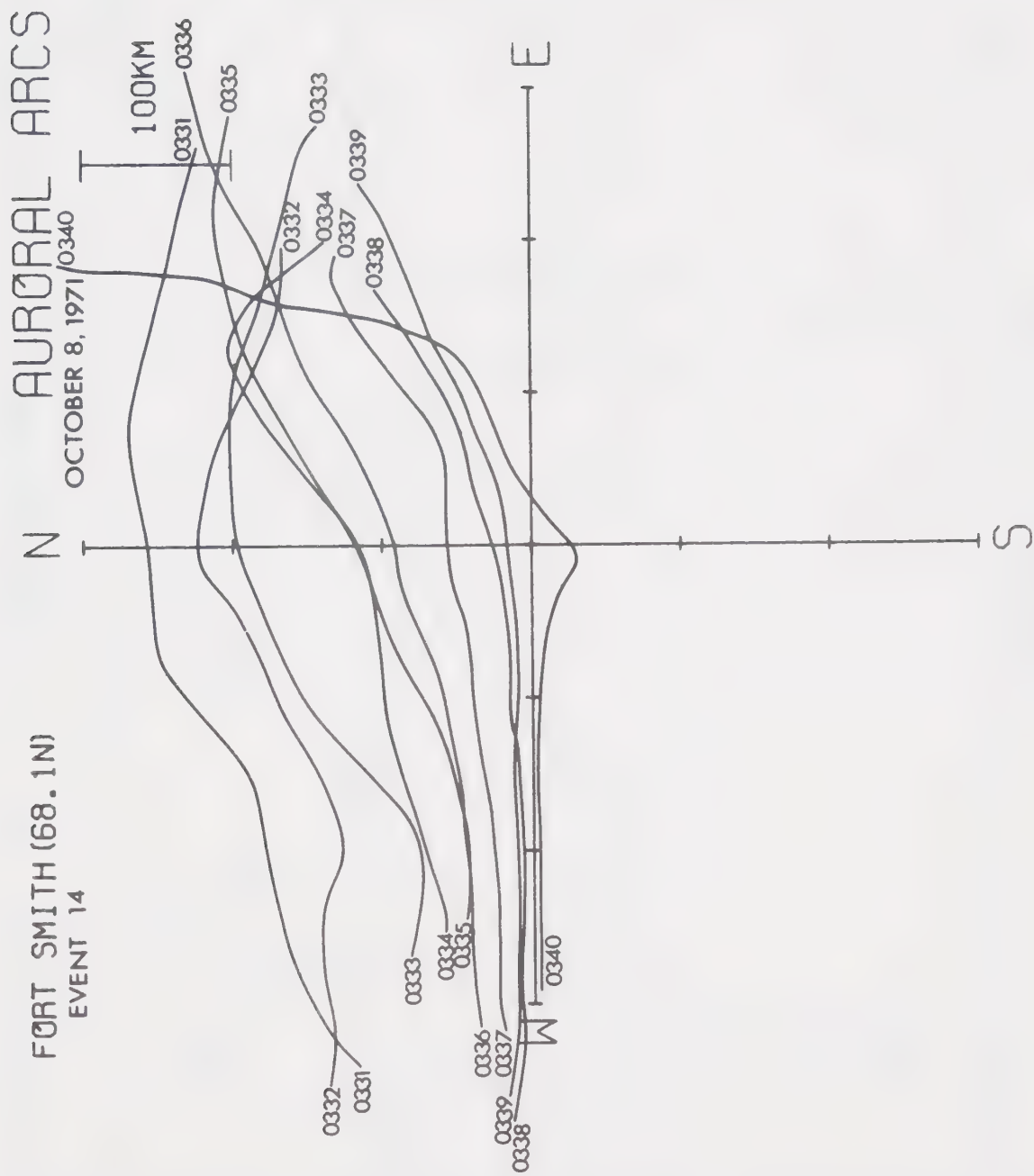


Figure A2b

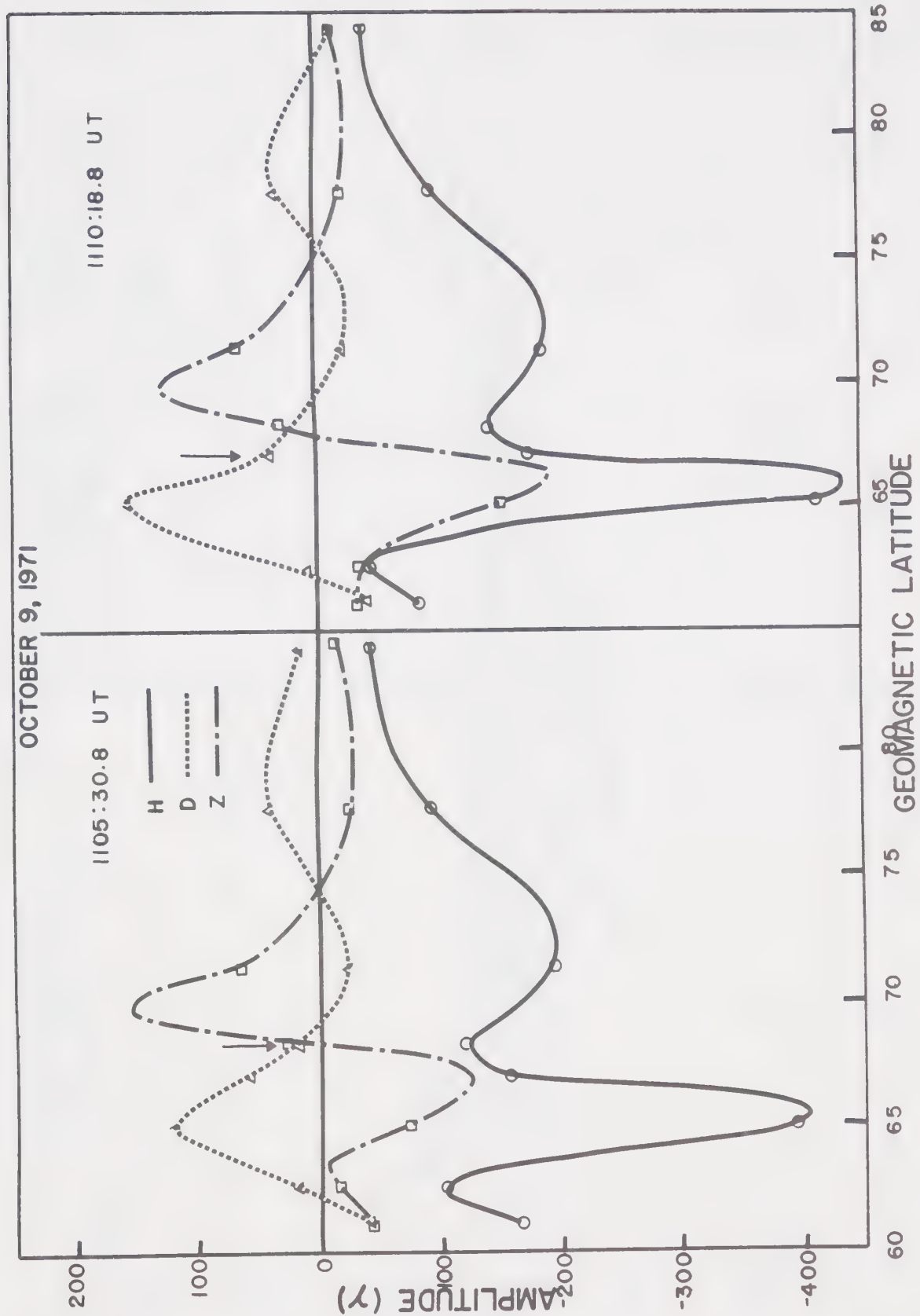


Figure A3a

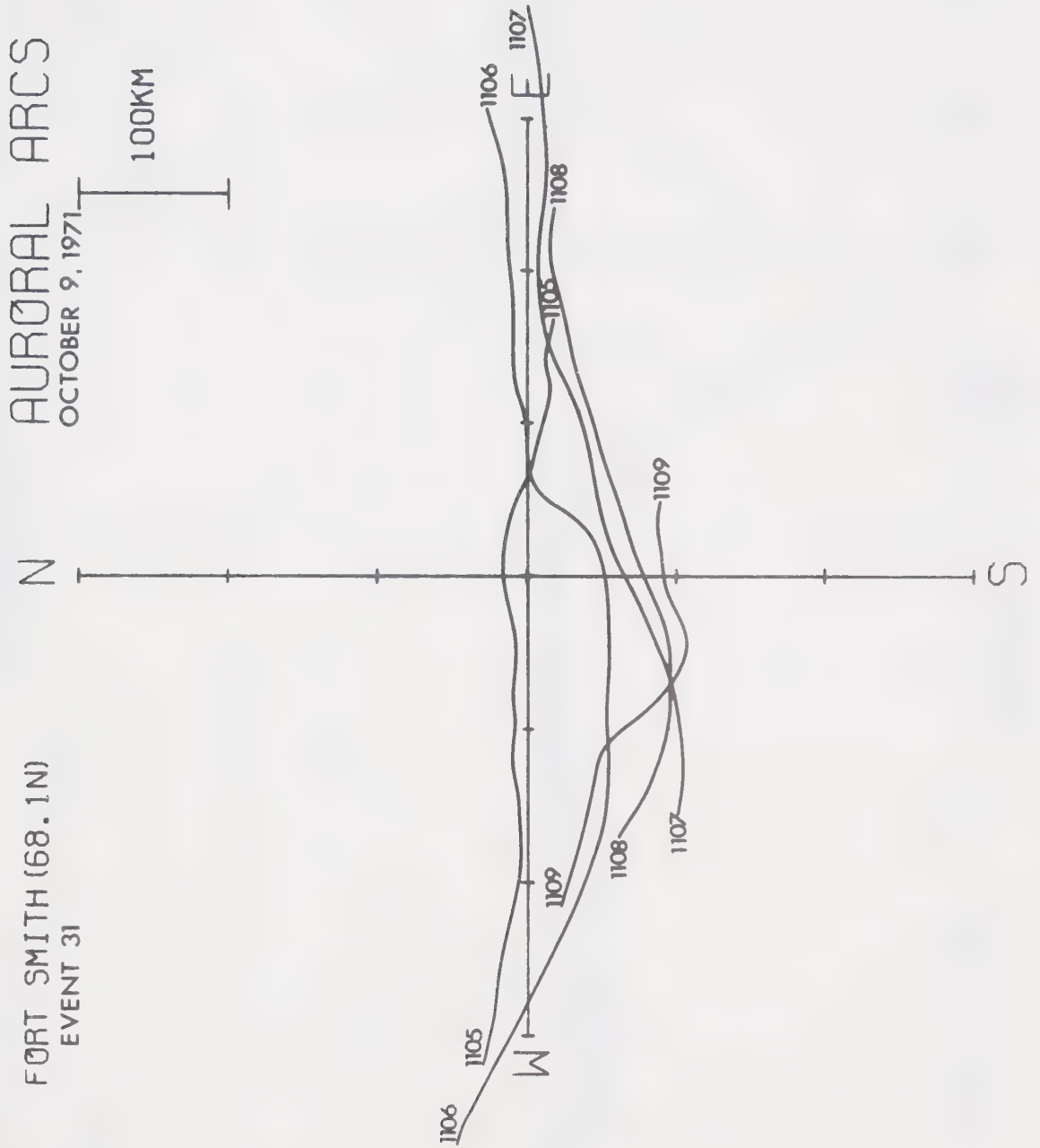


Figure A3b

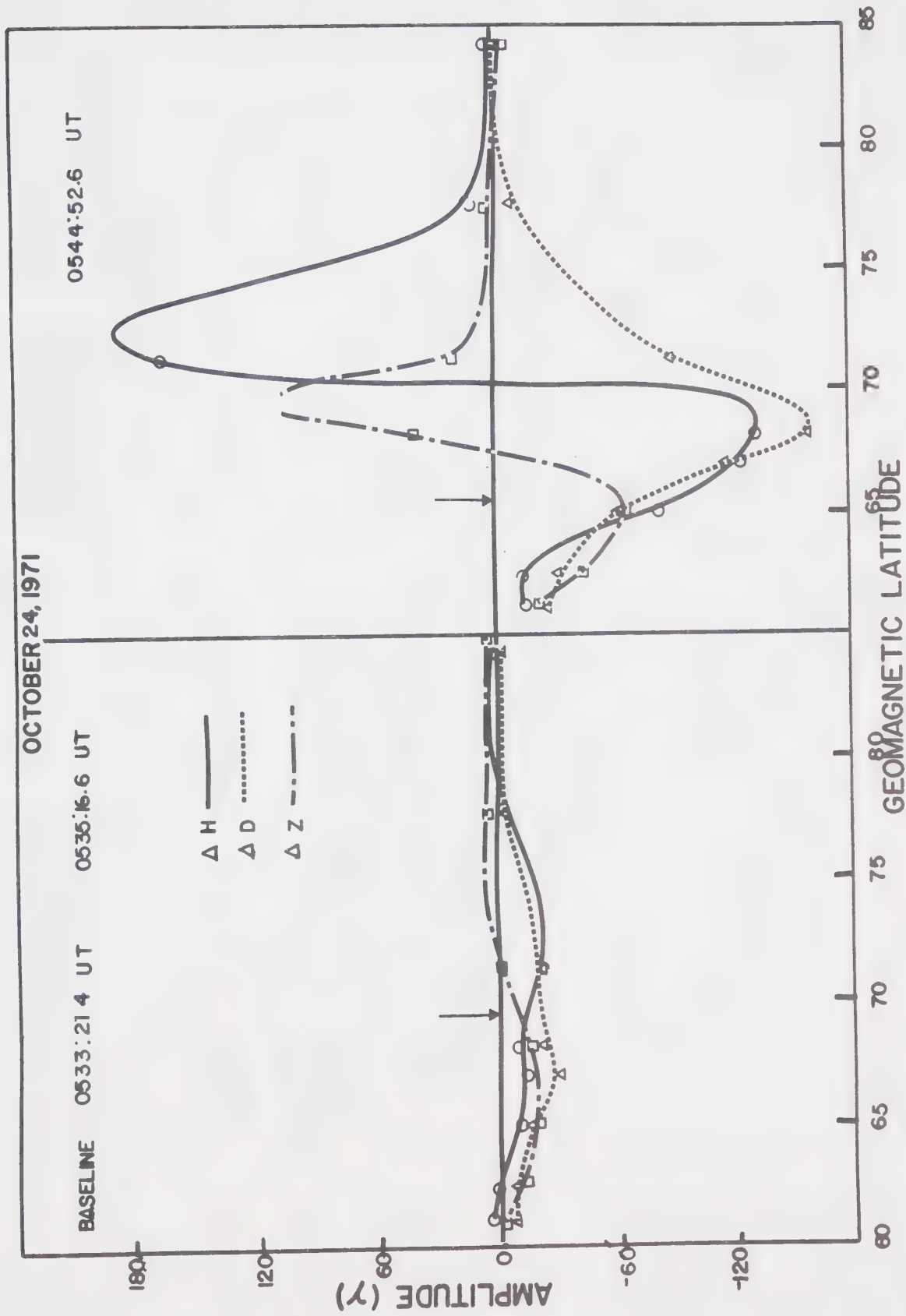


Figure A4a

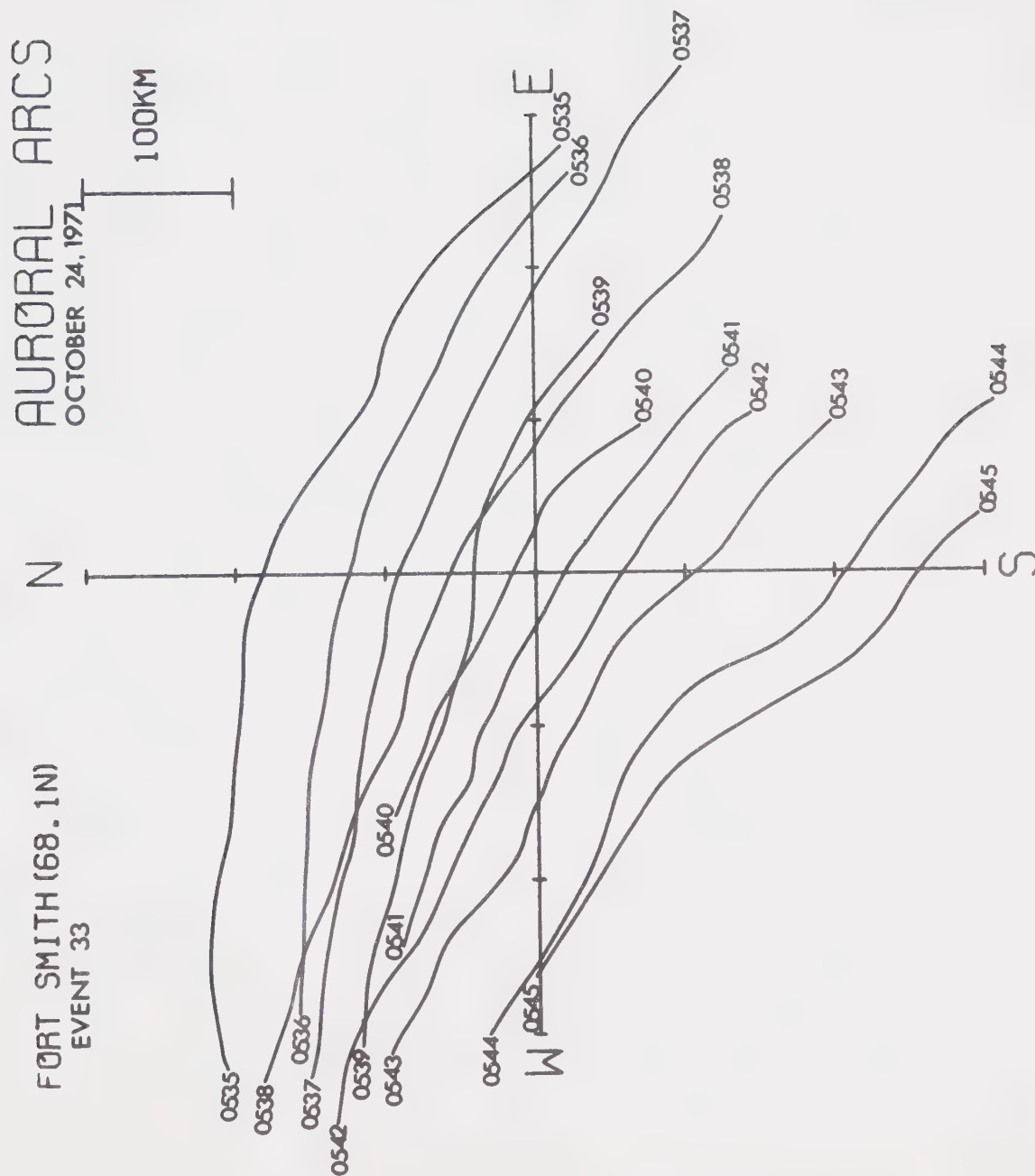


Figure A4b

B30034